Revisiting multifractality of high-resolution temporal rainfall using a wavelet-based formalism

V. Venugopal,[1,2] Stéphane G. Roux,[3] Efi Foufoula-Georgiou,[1] and Alain Arneodo[3]

Received 5 August 2005; revised 15 February 2006; accepted 9 March 2006; published 20 June 2006.

[1] We reexamine the scaling structure of temporal rainfall using wavelet-based methodologies which, as we demonstrate, offer important advantages compared to the more traditional multifractal approaches such as box counting and structure function techniques. In particular, we explore two methods based on the Continuous Wavelet Transform (CWT) and the Wavelet Transform Modulus Maxima (WTMM): the partition function method and the newer and more efficient magnitude cumulant analysis method. We also report the results of a two-point magnitude correlation analysis which is able to infer the presence or absence of multiplicativity as the underlying mechanism of scaling. The diagnostic power of these methodologies for small samples, signals with short ranges of scaling, and signals for which high-frequency fluctuations are superimposed on a low-frequency component (all common attributes of geophysical signals) is carefully documented. Application of these methodologies to several midwestern convective storms sampled every 5 s over several hours provides new insights. They reveal the presence of a very intermittent multifractal structure (a wide spectrum of singularities) in rainfall fluctuations between the scales of 5 min and the storm pulse duration (of the order of 1–2 hours for the analyzed storms). The two-point magnitude statistical analysis suggests that this structure is consistent with a multiplicative cascading mechanism which however is local in nature; that is, it applies only within each storm pulse but not over the whole storm duration.

Citation: Venugopal, V., S. G. Roux, E. Foufoula-Georgiou, and A. Arneodo (2006), Revisiting multifractality of high-resolution temporal rainfall using a wavelet-based formalism, *Water Resour. Res.*, *42*, W06D14, doi:10.1029/2005WR004489.

1. Introduction

[2] Analysis and modeling of space-time rainfall [e.g., *Schertzer and Lovejoy*, 1987; *Olsson et al.*, 1993; *Marsan et al.*, 1996; *Veneziano et al.*, 1996; *Cârsteanu and Foufoula-Georgiou*, 1996; *Venugopal and Foufoula-Georgiou*, 1996; *Harris et al.*, 1998; *Deidda et al.*, 1999; *Menabde and Sivapalan*, 2000] (see also *Foufoula-Georgiou* [1997] for a review) have been influenced by statistical theories of turbulence aiming at understanding the partition of energy at different scales. A breakthrough in the statistical theory of turbulence came about with the observation that the support of the transfer of energy is spatially intermittent, i.e., that the energy associated with the small scales in a turbulent flow is not distributed uniformly in space [*Meneveau and Sreenivasan*, 1991; *Frisch*, 1995]. This observation prompted a shift from the global Fourier-based analysis of Kolmogorov to a local analysis aimed at characterizing the nature of the very abrupt variations in velocity fluctuations. This led to the so-called multifractal formalism introduced by *Parisi and Frisch* [1985]. Loosely speaking, this formalism relates the scale dependence of the statistical moments of turbulent velocity fluctuations to the intermittent and multifractal nature of the points at which abrupt local increases of velocities exist.

[3] More specifically, *Parisi and Frisch* [1985] computed from experimental data, as a function of displacement ℓ, the average value of the qth power of the change in the turbulent velocity, that is, the average value of $|v(x+\ell) - v(x)|^q$ and found that it varied as power law $\ell^{\zeta(q)}$, where the exponent $\zeta(q)$ depended nonlinearly on q. They interpreted the nonlinear behavior of $\zeta(q)$ as an indication (or direct consequence) of the existence of spatial heterogeneity in the local regularity of the velocity field. Namely, by calling $D(h)$ the Hausdorff dimension of the set of points for which the increase in velocity acts as ℓ^h (points of singularity h), they showed that the contribution of these "singularities of order h" to the average value of $|v(x+\ell) - v(x)|^q$ is of the order of magnitude of the product $\ell^{qh} \cdot \ell^{1-D(h)}$; the second factor is the probability that a circle of radius ℓ intersects a fractal set of dimension $D(h)$. This forms the basis of the multifractal formalism, as one notes that when ℓ tends to 0, the dominant term in the above expression is the one with the smallest possible exponent, giving rise to the so-called Legendre transform $\zeta(q) = \inf_{h>0} [qh + 1 - D(h)]$. The nonlinearity of $\zeta(q)$ therefore indicates that the velocity

[1]St. Anthony Falls Lab, University of Minnesota, Minneapolis, Minnesota, USA.
[2]Now at Centre for Atmospheric and Oceanic Sciences, Indian Institute of Science, Bangalore, India.
[3]Laboratoire de Physique École Normale Supérieure, Lyon, France.

0043-1397/06/2005WR004489$09.00

fluctuations display multifractal scaling as characterized by a suite of h values given by $h(q) = \partial\zeta(q)/\partial q$.

[4] Having understood in a heuristic manner the intimate connection between $\zeta(q)$ and $D(h)$, we point out that the traditional multifractal analysis of turbulence [*Parisi and Frisch*, 1985; *Frisch*, 1995] or other geophysical signals, including rainfall, starts by estimating $\zeta(q)$ via a moment analysis (power law decay of $|v(x + \ell) - v(x)|^q$ with ℓ) and then estimating $D(h)$ from the Legendre transform. It is noted however, that to conclusively infer the nonlinearity of $\zeta(q)$ versus q, higher-order moments are typically needed which presents a problem for small sample sizes, or when the range of scaling is short. In addition, there are other shortcomings of this traditional methodology [*Muzy et al.*, 1993, 1994], such as the inability to access the whole range of singularity exponents, as will be discussed in detail in the following section.

[5] Motivated by recent advances in multifractal analysis of turbulence velocity signals [e.g., *Arneodo et al.*, 1998c, 1999; *Delour et al.*, 2001], this paper proposes to use an alternative methodology for diagnosing and estimating the multifractal structure of rainfall. The centerpiece of this estimation is access to the whole spectrum of singularities $D(h)$ which fully characterizes the intermittent structure of rainfall fluctuations and therefore the scaling of their statistical moments, or the scaling of the whole probability density function (PDF) using the so-called "propagator" method [*Castaing et al.*, 1990; *Arneodo et al.*, 1997b, 1998c]. As will be formally presented later, a natural tool for unraveling local singularities of a signal is the wavelet transform [e.g., *Muzy et al.*, 1994; *Mallat*, 1998] which acts as a microscope and by zooming locally at the signal can characterize the nature of its abrupt local fluctuations. A multifractal formalism based on wavelets has been well established in the turbulence literature [e.g., *Muzy et al.*, 1991; *Bacry et al.*, 1993; *Muzy et al.*, 1994; *Arneodo et al.*, 1995a], but has not been adequately explored yet for geophysical signals. One of the goals of this paper is to introduce the wavelet-based multifractal formalism [see also *Davis et al.*, 1994] and the related magnitude cumulant analysis method [*Delour et al.*, 2001] in a pedagogical way such that it can motivate further exploration of these powerful methodologies in geophysics. In particular, we will emphasize the investigation of the correlations of the logarithms of the wavelet coefficients (the so-called "magnitude") as a powerful test of the existence of a possible underlying multiplicative structure [*Arneodo et al.*, 1998a, 1998b]. The second goal is to revisit the multiscaling analysis of high-resolution temporal rainfall and offer new insights on its multifractal structure.

[6] The paper is structured as follows. In section 2 we present a brief but self-contained review of the wavelet-based multifractal formalism. We start with the continuous wavelet transform and show how it can be used to extract singularities of a signal. We then demonstrate that by concentrating on critically selected points only (the maxima lines pointing to singularities), i.e., working with the Wavelet Transform Modulus Maxima (WTMM) coefficients, results in a more robust estimate of the singularity spectrum $D(h)$. We also note that by using the WTMM coefficients instead of the CWT coefficients, we have access to the whole range of singularities including the decaying part of the $D(h)$ curve, which can only be resolved by computing the scaling of negative moments (not possible in the typical structure function or CWT multifractal analysis as the PDFs of those fluctuations are centered around zero). In section 3 we introduce the one- and two-point cumulant analysis method and explain its advantages versus the CWT and WTMM standard multifractal analysis. In section 4 we present the results of applying the proposed methodology to four high-resolution storms sampled every 5 s over the midwestern U.S. For illustrative purposes we present and compare the results of the structure function, CWT, WTMM and cumulant analysis on one data set. We pay special attention to using wavelets of increasing order, i.e., increasing number of vanishing moments, to (1) properly remove nonstationarities in the signal and define (instead of impose) the "fluctuations" whose scaling properties we characterize and (2) to have confidence that the scaling behavior and scaling exponent estimates do not depend on the chosen wavelet. Section 5 presents the results of a timescale magnitude correlation analysis of rainfall fluctuations and poses the hypothesis of a local (within storm pulse) multiplicative cascade. This hypothesis is further tested via a numerical experiment. Section 6 presents the theory of probability density function rescaling via the so-called "propagator" approach and demonstrates its application to the rainfall intensity series. A summary of the inferences about the multiscaling structure of temporal rainfall and concluding remarks are made in section 7.

2. Wavelet-Based Multifractal Formalism

2.1. Spectrum of Singularities

[7] The traditional multifractal formalism was developed in the framework of dynamical systems for the description of the scale-invariant properties of singular measures [*Halsey et al.*, 1986; *Collet et al.*, 1987; *Paladin and Vulpiani*, 1987]. The formalism is based on the mathematical concept of a measure μ on $\mathcal{R}$ which is only defined under an integral over an arbitrary subset $\mathcal{S}$ of $\mathcal{R}$: $\mu(\mathcal{S}) = \int_{x\in\mathcal{S}} d\mu(x)$. A good example is the Dirac measure (not actually a "function") $\int_{x_1}^{x_2} \delta(x)\, dx = 1$ if $x_1 < 0$ and $x_2 > 0$ and 0 otherwise. The singularity exponent $\alpha(x_0)$ at a point x_0 of a measure μ (on $\mathcal{R}$) is then defined as:

$$\alpha(x_0) = \lim_{\epsilon\to 0^+} \frac{\ln \mu(B_{x_0}(\epsilon))}{\ln \epsilon}, \tag{1}$$

where $B_{x_0}(\epsilon)$ is a "box" of size ϵ centered around x_0. The exponent $\alpha(x_0)$ represents the singularity "strength" of the measure μ at x_0. The smaller the value of $\alpha(x_0)$, the more singular the measure. The limit $\alpha = 0$ corresponds to a behavior similar to a Dirac distribution at x_0. The spectrum of singularities $\mathcal{F}(\alpha)$ of the measure μ is defined as the fractal (more precisely, Hausdorff) dimension of the set of all points x_0 such that $\alpha(x_0) = \alpha$:

$$\mathcal{F}(\alpha) = d_H\{x_0 \in \text{Support of } \mu, \alpha(x_0) = \alpha\}. \tag{2}$$

The singularity spectrum describes the statistical contribution of the singularity exponents $\alpha(x)$. Thus a measure is monofractal, if it has the same singularity exponent, α_0, throughout its support, and the singularity spectrum is a

point at (α_0, $\mathcal{F}(\alpha = \alpha_0) = D_f$), where D_f is the fractal dimension of the support of the singularities of the measure. A multifractal measure, on the other hand, has singularities of different strengths (orders) throughout its support, and the resulting singularity spectrum is a concave function (a "bump") with the maximum at the most frequently occurring singularity.

[8] The concept of singularity exponent α for measures has a natural counterpart for functions, which is called the Hölder exponent, h, defined as [*Muzy et al.*, 1994; *Mallat*, 1998]:

$$|f(x_0) - f(x_0 + \epsilon)| \sim C|\epsilon|^{h(x_0)}, \tag{3}$$

where $h(x_0)$ characterizes the singularity of the function f at x_0. As $h \to 0$, the function becomes more singular (i.e., less regular). By definition, $0 \leq h < 1$, with the limits $h = 0$ corresponding to a discontinuity (e.g., step function), and $h = 1$ corresponding to a discontinuity in the derivative (e.g., integral of a step function). The similarity of equation (3) to (1) can be easily seen. While equation (1) refers to a box of size ϵ around a point, equation (3) refers to the "change" of a function from a point to another point ϵ "distance" away. In other words, integrals/sums in "boxes" are replaced by "increments." Similar to the definition of the singularity spectrum $\mathcal{F}(\alpha)$, one can define a spectrum of Hölder exponents $D(h)$, as the Hausdorff dimension d_H of the set of all points x such that $h(x) = h$ [*Parisi and Frisch*, 1985; *Bacry et al.*, 1993; *Muzy et al.*, 1994; *Jaffard*, 1997]. That is,

$$D(h) = d_H\{x \in \text{ support of } f(x), h(x) = h\}. \tag{4}$$

One could generalize the definition in equation (3), to functions for which singularities of higher orders ($h > 1$) exist; that is, singularities exist in the higher-order derivatives of the function. Thus a generalized definition of the Hölder exponent, $h(x_0)$ is [*Muzy et al.*, 1994; *Arneodo et al.*, 1995a]:

$$|f(x) - P_n(x - x_0)| \leq C|x - x_0|^{h(x_0)}. \tag{5}$$

In words, $h(x_0)$ is the largest exponent such that there exists a polynomial $P_n(x)$ of order n that satisfies the above condition in the neighborhood of x_0. For example, $h(x_0) = 0.7$ implies that the function $f(x)$ is not differentiable at x_0 and $h(x_0) = 1.3$ implies that the function is differentiable at x_0, but its derivative is not, i.e., that the singularity lies in the second derivative of the function. Thus, if we have a function whose n^{th} derivative is singular, then $g(x) = d^n f(x)/dx^n$ is singular with $0 < h_g < 1$. This implies $f(x)$ has a singularity exponent $h_f = h_g + n$, or, $n < h_f < n + 1$. Note that this is because of the fact that differentiation reduces the regularity order by 1 and integration increases it by 1, as long as the function does not possess oscillatory singularities [*Arneodo et al.*, 1995b; *Arneodo et al.*, 1997a]. In this study we will implicitly assume that all singularities are cusp shaped. As mentioned before (equation (4)), by collecting all the points x at which the local Hölder exponent is equal to h, and computing the Hausdorff dimension $D(h)$ of this set of points, one can obtain its singularity spectrum $D(h)$. We now have a generalized framework wherein singularities (of any order) of functions can be characterized by the exponent h, where $0 \leq h < \infty$, and its spectrum $D(h)$.

[9] Furthermore, the above framework can be extended to singular measures by defining the Hölder exponent h as $h = \alpha - 1$, where α is defined in equation (1). Since $\alpha > 0$, this amounts to allowing the Hölder exponent to take values $h \geq -1$. Thus, in the unified framework for defining singularities for distributions, including measures and functions, $D(h)$ represents the singularity spectrum with $-1 \leq h < \infty$. In the rest of the discussion, we use h and $D(h)$. We refer the reader to the end of section 2.4 for a discussion on the properties of $D(h)$. We now show that the wavelet transform provides an appropriate framework for adaptively incorporating the singularity properties of both "sums in boxes" as well as the "increments."

2.2. Extraction of Singularities Using Wavelet Transforms

[10] The continuous wavelet transform of a function $f(x)$ can be defined as:

$$T_\psi[f](b, a) = \frac{1}{|a|}\int f(x)\psi\left(\frac{x - b}{a}\right)dx, \qquad a > 0, b \in R, \tag{6}$$

where a is the scale parameter, and b is the location parameter. ψ defines a family of wavelets; that is, for varying values of a, wavelets of different length scales can be constructed. (For a general reference on wavelets, see *Meyer* [1992], *Daubechies* [1992], and *Mallat* [1998].) The wavelet transform can be seen as decomposing the function $f(x)$ into elementary space-scale contributions by convolving it with a suite of localized (space/time and scale/frequency) functions, the so-called wavelets, all of which are constructed by translation and dilation of a single function, the analyzing or "mother" wavelet. Note that in equation (6), we have used an $\mathcal{L}^1$ norm ($\frac{1}{|a|}$). The classical definition [*Meyer*, 1992; *Daubechies*, 1992] defines it with an $\mathcal{L}^2$ norm ($\frac{1}{|a|^{1/2}}$). Depending on the application, there are a variety of ways of computing the wavelet transform. For instance, for the purpose of compact representation (compression), one could compute an orthogonal wavelet transform on dyadic scales (multiresolution framework introduced by *Mallat* [1989]). For the study of self-similar processes (fractals), continuous wavelet transforms have been found to be effective [*Arneodo et al.*, 1988, 1995a; *Muzy et al.*, 1994].

[11] An attractive feature of wavelets is that one could construct various analyzing patterns (which satisfy the requirements for a function to be called a wavelet; see *Daubechies* [1992]) depending on the application. On the one hand, when periodic functions are to be analyzed, or when the objective is to localize a time-dependent frequency, or when there are characteristic (temporal or spatial) scales present in the phenomenon under study, a complex wavelet (e.g., Morlet wavelet) is better than a real wavelet (e.g., Mexican hat wavelet [*Meyer*, 1992; *Daubechies*, 1992; *Mallat*, 1998]. On the other hand, when the underlying process does not have characteristic scales, or when the goal is to identify discontinuities or singularities, a real wavelet is more appropriate [*Muzy et al.*, 1994; *Mallat*, 1998]. In this work, we use the successive derivatives of a Gaussian function:

$$g^{(N)}(x) = \frac{d^N}{dx^N}e^{-x^2/2}, \tag{7}$$

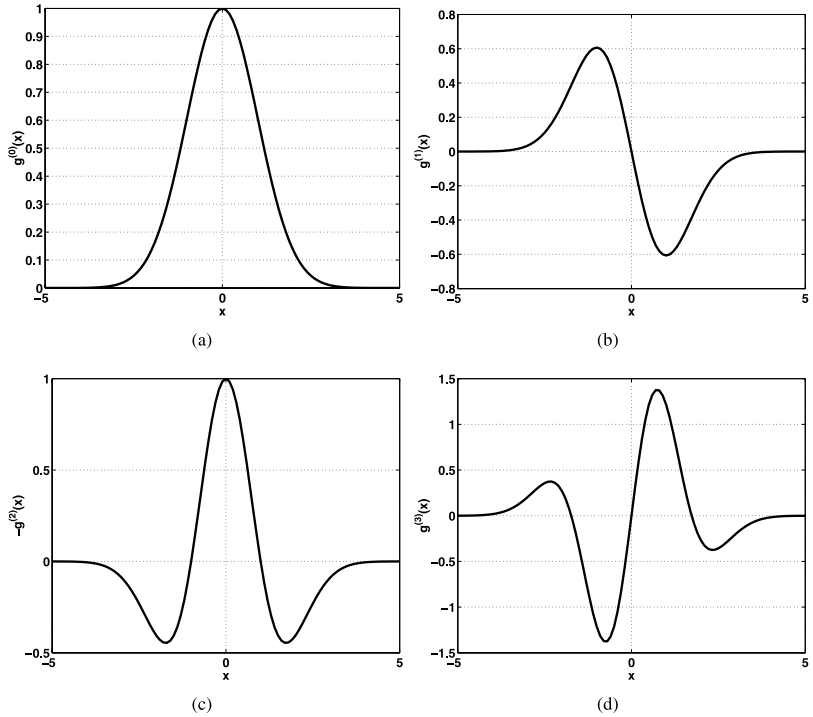

Figure 1. Derivatives of the Gaussian, $g^{(N)}(x)$ (equation (7)), for (a) $N = 0$, (b) 1, (c) 2, and (d) 3.

which have been extensively used, as a smooth generalization of Nth-order increments, to study the behavior of fractal functions [*Muzy et al.*, 1994; *Arneodo et al.*, 1995a]. It is easy to see (Figure 1) that $g^{(0)}(x)$, a Gaussian function, is equivalent to the "box" function (used to compute the singularities of a measure) and $g^{(1)}(x)$ is equivalent to the "increment" (structure function used for computing singularities in a function which is continuous, but not differentiable). $g^{(2)}(x)$ is the well-known "Mexican hat" wavelet. These functions ($g^{(N)}(x)$) are well localized in both space and frequency, and more importantly, the property of the (first) N vanishing moments of $g^{(N)}(x)$, i.e.,

$$\int_{-\infty}^{\infty} x^q g^{(N)}(x)dx = 0,\ 0 \le q < N, \tag{8}$$

proves to be a very useful property in extracting singularities, as discussed below.

[12] It has been shown [*Jaffard*, 1989; *Holschneider and Tchamitchian*, 1990; *Mallat and Hwang*, 1992] that by using an analyzing wavelet ψ which has n_ψ vanishing moments, the behavior of $T_\psi[f](x_0, a)$ as a function of scale, a, as $a \to 0$ characterizes the local behavior of $f(x)$ in equation (5), i.e.,

$$T_\psi[f](x_0, a) \sim a^{h(x_0)} \qquad a \to 0, \tag{9}$$

provided $n_\psi > h(x_0)$. In other words, the local singular behavior of f around x_0 is characterized by a power law behavior (with an exponent $h(x_0)$) of the wavelet transform of f at the point x_0, as a function of scale, a, as $a \to 0$. If $h(x_0)$ is positive and small (implying that the function is singular), then we can visualize this as a slow decay of wavelet coefficients with scale; if $h(x_0)$ is large and positive (implying that the function is regular) [see *Jaffard*, 1989; *Holschneider and Tchamitchian*, 1990], then the wavelet coefficients decay rapidly as a function of scale. If $h(x_0) < 0$, then the wavelet coefficients, instead of decaying, increase with scale [*Roux et al.*, 1999]. Thus the more singular the function at a given location, the larger the wavelet coefficients at that location at small scales.

[13] A remark on the choice of the order of wavelet is in order. Note that in equation (9), n_ψ, the number of vanishing moments of the wavelet *must be greater than* $h(x_0)$ in order to be able to resolve this singularity. If one were to choose a wavelet with $n_\psi < h(x_0)$, then the resulting decay of wavelet coefficients would be at a rate equal to n_ψ giving a misleading estimate of $h(x_0)$ equal to n_ψ [*Bacry et al.*, 1993; *Muzy et al.*, 1994]. Therefore to resolve all singularities present in a function, the analyzing wavelet must be chosen to have $n_\psi \ge h_{\max}$ where $h_{\max}$ is the weakest singularity present in the function. Since $h_{\max}$ is not known a priori, the most appropriate way to correctly estimate all singularities is to analyze the given function with wavelets of increasing order (i.e., increasing number of vanishing moments). If for order n_ψ and $n_\psi + 1$, one gets the same $D(h)$ curve, then it can be assured that n_ψ (or $n_\psi + 1$) is the right order of the wavelet. It is noted that the convolution of $f(x)$ with a wavelet of order $(n_\psi + 1)$ can be shown to remove polynomial trends of order n_ψ [e.g., see *Muzy et al.*, 1994]. This implies that if a wavelet of degree $(n_\psi + 1)$ is accepted as the one resulting in a robust estimate of $D(h)$, this wavelet has also filtered out nonstationarities of polynomial type of degree n_ψ from the function. In other words, the wavelet coefficients $T_\psi[f]$ can be assumed stationary and their statistical moments safely computed. This is important

since it is these moments that form the basis of estimating $D(h)$ as explained in the next section.

2.3. $D(h)$ Estimation Using CWT

[14] Having seen the ability of the continuous wavelet transform to capture singularities of all orders ($<\infty$), we turn our attention to the specific task of estimating the singularity spectrum, $D(h)$, and the intricacies involved therein. As originally proposed by *Holschneider* [1989] and further used by *Muzy et al.* [1994], one can define a "partition function" $Z(q, a)$ from the wavelet coefficients:

$$Z_{\mathrm{cwt}}(q,a) = \int |T_\psi[f](x,a)|^q dx, \tag{10}$$

that can be shown to behave for a multifractal process, as

$$\mathcal{Z}_{\mathrm{cwt}}(q,a) \sim a^{\tau_{\mathrm{cwt}}(q)} \qquad a \to 0, q > 0. \tag{11}$$

Then by taking the Legendre transform of $\tau_{\mathrm{cwt}}(q)$, one can compute the singularity spectrum $D(h)$ [*Muzy et al.*, 1994].

$$D(h) = \min_q \left[qh - \tau_{\mathrm{cwt}}(q) + D_f\right], \tag{12}$$

where D_f is the fractal dimension of the support of singularities of f. For the case of a continuously differentiable $\tau_{\mathrm{cwt}}(q)$, the following relations hold:

$$\begin{aligned} q &= dD/dh, \\ \tau_{\mathrm{cwt}}(q) &= qh - D(h) + D_f, \end{aligned} \tag{13}$$

and, equivalently

$$\begin{aligned} h &= d\tau_{\mathrm{cwt}}/dq, \\ D(h) &= qh - \tau_{\mathrm{cwt}}(q) + D_f. \end{aligned} \tag{14}$$

Although this methodology provides an improvement to the standard structure function-based multifractal formalism [*Parisi and Frisch*, 1985; *Frisch*, 1995], it still has a couple of critical shortcomings [see also *Muzy et al.*, 1993].

[15] 1. First, if one takes a continuous sum of the wavelet coefficients (see equation (10)) to estimate the partition function, the number of points used in the summation remains the same irrespective of the scale. In other words, for $q = 0$, the partition function is independent of scale, and equal to the number of samples in the given data set, i.e., $Z_{\mathrm{cwt}}(0, a)$ = constant $\sim a^{\tau_{\mathrm{cwt}}(0)}$. This, in turn, implies that $\tau_{\mathrm{cwt}}(0) = 0$ trivially, and thus by using all the wavelet coefficients, it is not possible to estimate the fractal dimension D_f of the support of singularities. For example, for the "Devil's staircase" the method would give $D_f = 1$ instead the true fractal dimension of ln 2/ln 3 (the fractal dimension of the triadic Cantor set). This shortcoming prompts the explicit introduction of D_f (which needs to be estimated by other methods) in equations (12)–(14).

[16] 2. Second, note that the probability density function of the wavelet coefficients is finite (if not maximum) at zero. This presents a problem for $q < 0$, because the partition function $Z(q, a)$ would diverge. Similar to the problem that one encounters with a first-order structure function, one cannot estimate the right side (decreasing limb) of the $D(h)$ spectrum (see Figure 2), which corresponds to $q < 0$ [*Muzy et al.*, 1993, 1994]. Note however that the difference between the structure function approach and the CWT-based approach described above is that while the former approach (at least, first-order increments) cannot estimate $h > 1$, the latter approach, using higher-order wavelets systematically, can estimate $h > 1$, as long as those values of h are to the left of $\langle h \rangle$ where the maximum value of the $D(h)$ spectrum is achieved. For practical purposes however, one cannot take advantage of this unless the function analyzed has a mean singularity $\langle h \rangle$ greater than 1. This will be discussed later in the context of the rainfall data analysis.

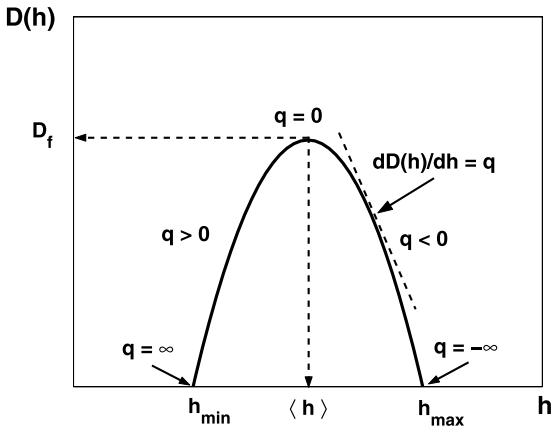

Figure 2. Generic shape of the $D(h)$ singularity spectrum considered as the Legendre transform of $\tau(q)$.

[17] On the basis of the above discussion, it is seen that estimation of $D(h)$ based on the partition function presented in equations (10)–(14) (which is the classical multifractal formalism extended via wavelets) has the limitation that only part of the singularity spectrum, i.e., the rising limb of $D(h)$ corresponding to $q > 0$, can be captured. To be able to take negative moments and to estimate the complete singularity spectrum, *Muzy et al.* [1991, 1993, 1994] proposed to use the wavelet transform modulus maxima (WTMM) method.

2.4. $D(h)$ Estimation Using WTMM

[18] The Wavelet Transform Modulus Maxima (WTMM) are defined at each scale a as the local maxima of $|T_\psi[f](x, a)|$ considered as a function of x [*Mallat and Hwang*, 1992; *Mallat*, 1998]. These WTMM form connected curves, called maxima lines and contain information about the hierarchical structure of singularities. In fact, each time the function $f(x)$ has a local Hölder exponent $h(x_0) < n_\psi$ at the point x_0, there are $n_\psi + 1$ lines pointing toward x_0 along which equation (9) is true (for example, if the first derivative of the Gaussian is used, the two extrema in the analyzing function $g^{(1)}(x)$ (see Figure 1) would manifest themselves as modulus maxima in the wavelet coefficient timescale plane). The partition function defined in equation (10) can then be modified such that it is computed only on the wavelet transform skeleton [*Muzy et al.*, 1991, 1994; *Bacry et al.*, 1993] as:

$$\mathcal{Z}_{\mathrm{wtmm}}(q,a) = \sum_{\ell \in \mathcal{L}(a)} \left[|T_\psi[f](x,a)|\right]^q, \tag{15}$$

where $q \in \mathcal{R}$, $\mathcal{L}(a)$ is the set of all maxima lines ℓ that satisfy: $\ell \in \mathcal{L}(a)$, if $\forall\ a' \leq a$, $\exists (x, a') \in \ell$.

[19] The definition of $\mathcal{Z}_{\mathrm{wtmm}}(q, a)$ in equation (15), implies that the summation is done over "well chosen" points (scale-adaptive partition via the WTMM) rather than taking a "blind" global average over the whole length of the signal. *Muzy et al.* [1993, 1994] found that even this definition is not fully equipped with the ability to provide reliable and complete estimates of the scaling exponents spectrum ($\tau(q)$) and the singularity spectrum ($D(h)$). The particular case where this aforementioned formulation can diverge is when the maximum value of the modulus of the wavelet transform is very small in value. In such a case, for $q < 0$, there could potentially be numerical instabilities in the computation of the partition function. To alleviate this concern, *Muzy et al.* [1993, 1994] reformulated the definition of the partition function in equation (15) by replacing the value of the wavelet transform modulus at each maximum by the supremum value along the corresponding maxima line at scales smaller than a:

$$\mathcal{Z}_{\mathrm{wtmm}}(q,a) = \sum_{\ell \in \mathcal{L}(a)} \left[\sup_{(x,a') \in \ell,\ a' < a} |T_\psi[f]\left(x, a'\right)| \right]^q, \qquad (16)$$

where the "sup" is a way of preventing divergence in the computation of $\mathcal{Z}(a, q)$ for negative q values [*Bacry et al.*, 1993]. In this procedure, one traverses along a maxima line ($\mathcal{L}(a)$) from the largest to smallest scale, and at each scale (say a_1), replaces the value of the modulus maxima of the wavelet transform with a value that corresponds to the maximum for all scales $a < a_1$ along that maxima line. In our analysis, this was the estimation procedure used. There is however a drawback with computing the sup. If there are any singularities with negative Hölder exponent present in the signal, i.e., $h < 0$, recall that the modulus of the wavelet transform of the signal does not decay, but increases from large to small scales. Thus, if one were to replace the modulus maxima with *sup* along a maxima line, that would result in a horizontal maxima line, which would mean a trivial incorrect value of zero for the strength of the singularity.

[20] The inability of the "WTMM with sup" methodology to access negative singularities ($h < 0$) can easily be circumvented by working with the cumulative (or integral) of the signal of interest. Recall that integration adds 1 to the (cusp like) singularities of the signal, that is, it shifts $D(h)$ to the right by 1. Therefore singularities $-1 < h < 0$ in a signal would become singularities $0 < h < 1$ in the cumulative, posing no estimation problem in the "WTMM with sup" method. Once the spectrum of singularities of the cumulative signal, denoted by $D_c(h)$, is estimated, then

$$D(h) = D_c(h + 1). \qquad (17)$$

[21] Unless otherwise specified, for the rest of the discussion, the subscript *wtmm* implicitly includes the *sup*, i.e., $\mathcal{Z}_{\mathrm{wtmm}}$ computed from equation (16). The multifractal formalism then involves [see *Muzy et al.*, 1994]

$$\mathcal{Z}_{\mathrm{wtmm}}(q,a) \sim a^{\tau_{\mathrm{wtmm}}(q)} \qquad a \to 0, q \in \mathcal{R}, \qquad (18)$$

and, by taking the Legendre transform of $\tau_{\mathrm{wtmm}}(q)$, the singularity spectrum $D(h)$ results (see Figure 2):

$$D(h) = \min_q [qh - \tau_{\mathrm{wtmm}}(q)]. \qquad (19)$$

[22] Similarly, for the case of a continuously differentiable $\tau_{\mathrm{wtmm}}(q)$, the following relations hold:

$$\begin{aligned} q &= dD/dh, \\ \tau_{\mathrm{wtmm}}(q) &= qh - D(h), \end{aligned} \qquad (20)$$

and, equivalently

$$\begin{aligned} h &= d\tau_{\mathrm{wtmm}}/dq, \\ D(h) &= qh - \tau_{\mathrm{wtmm}}(q). \end{aligned} \qquad (21)$$

A few important points to be noted about this formalism are as follows [*Muzy et al.*, 1993, 1994; *Bacry et al.*, 1993; *Arneodo et al.*, 1995a]:

[23] 1. Unlike the case of the partition function computation using the continuous wavelet transform, we note that with WTMM, $\tau(0)$ can also be computed, because by summing over only the maxima lines, for $q = 0$, one would see how the number of maxima lines changes with scale, i.e., a^{-D_f}, where D_f is the fractal dimension of the support of the singularities. Furthermore, for $q < 0$, there is no concern of divergence, since the PDF of the WTMM coefficients decreases to zero at zero whatever the scale (at least in the limit of infinitely long signal), and $\tau(q)$ for $q < 0$ characterizes the way this decrease evolves across scale. Thus, using WTMM, one has access to the entire singularity spectrum, namely its increasing as well as its decreasing limbs.

[24] 2. If one were to choose a Gaussian function as the analyzing wavelet ($g^{(0)}(x)$), the WTMM method and the classical box counting method would be similar. Recall that the box counting methodology for singular measures only takes into account those boxes which have "mass," and which contain singularities [*Halsey et al.*, 1986; *Paladin and Vulpiani*, 1987; *Grassberger et al.*, 1988; *Meneveau and Sreenivasan*, 1991]. Summing over the maxima lines achieves exactly the same objective, since the maxima lines converge to the support of the singularities of the function. However, they are not exactly identical in the sense that the partition function from the WTMM has a scale (a) as a normalization factor (coming from the definition of the wavelet transform, see equation (6)). Thus $a^q\ \mathcal{Z}_{\mathrm{wtmm}}(q, a) = \mathcal{Z}_{\mathrm{box}}(q, a)$. This implies $\tau_{\mathrm{box}}(q) = \tau_{\mathrm{wtmm}}(q) + q$. Taking the Legendre transform on both sides, it can be easily shown that $D(h)$ (from WTMM) is equal to $\mathcal{F}(h + 1)$ (from box counting), where $\mathcal{F}(\alpha)$ is the singularity spectrum that one typically obtains with a box counting methodology. Thus the singularity spectrum for the box counting is shifted by 1 in the WTMM formalism [*Muzy et al.*, 1994].

[25] 3. For the sake of completeness, we mention here some well-known facts about $\tau(q)$ and $D(h)$ [*Muzy et al.*, 1994] where, from here on, we drop the subscript "wtmm." First, $\tau(0)(= -D_f)$, as mentioned before, captures the fractal dimension of the support of the function. Moreover, it is easy to see that the maximum value of $D(h)$ is at q = 0

(equation (20)), with the value of $h = \langle h \rangle$ being the most frequently occurring singularity and $D(h)$ equal to the fractal dimension of the support. $\tau(1)$ is related to the dimension of the graph of the given function ($d_{\mathcal{G}} = \max(1, 1 - \tau(1))$); and $\tau(2)$, also called the correlation dimension, is related to the scaling exponent of the Fourier spectral density ($|\hat{f}(\omega)|^2 \sim \omega^{-\beta}$), by the relation $\tau(2) = \beta - 2$. $D(h)$ is a convex function, whose tangents (dD/dh) give the values of the order of the moment, q. In addition, one can deduce that $q < 0$ is mapped to the right of the maximum $D(h)$, and $q > 0$ is mapped to the left of the maximum. From equation (20), one can also deduce that $h_{\max}$ corresponds to $q = -\infty$ and $h_{\min}$ corresponds to $q = +\infty$ (see Figure 2).

[26] 4. From the Legendre transform properties (equations (19)–(21)), it is clear that the signature of monofractality, i.e., the existence of a unique Hölder exponent, $h = H$, will be a linear $\tau(q)$ spectrum of slope H. Multifractality, i.e., the existence of a finite range of $h = [h_{\min}, h_{\max}]$, will manifest as a nonlinear behavior of $\tau(q)$ versus q.

3. Cumulant Analysis Method

[27] In the multifractal formalism presented in the previous section, the process of obtaining the singularity spectrum involves fitting straight lines, if appropriate, to the log-log plots of the partition function $Z(q, a)$ versus scale a for different order moments q. Each value of q yields a value of the slope $\tau(q)$. To be able to define the entire $\tau(q)$ curve (and subsequently h and $D(h)$ via a Legendre transform), one needs to be able to fit many straight lines for a large range of q values and then proceed to fit a $\tau(q)$ curve to the resulting slopes of the straight lines, prior to the Legendre transform. While this has been the traditional way of estimating $\tau(q)$ and $D(h)$, recently in the turbulence literature [*Delour*, 2001; *Delour et al.*, 2001], an alternate method, based on cumulants, was introduced which involves fitting only a few lines (as low as 3) while still adequately inferring and accurately estimating the nonlinear behavior of the spectrum of scaling exponents $\tau(q)$. This method is based on cumulants and is described below.

3.1. Magnitude Cumulant Analysis

[28] Let X be a random variable and $\mathcal{P}(x)$ its probability density function. The moment generating function (or characteristic function) defined as

$$\Phi_p(k) \equiv \int_{-\infty}^{\infty} e^{ikx} \mathcal{P}(x) dx, \tag{22}$$

can be shown via Taylor series expansion to take the form

$$\Phi_p(k) = \langle e^{ikx} \rangle = \sum_{n=0}^{\infty} M_n \frac{(ik)^n}{n!}, \tag{23}$$

where M_n is the nth-order moment of X

$$M_n = \int_{-\infty}^{\infty} x^n \mathcal{P}(x) dx, \qquad n = 0, 1, 2, \cdots \tag{24}$$

In other words, the moments M_n result by taking the n^{th} derivative of $\Phi_p(k)$ at $k = 0$. Similarly, the cumulant generating function of X is defined as

$$\Psi_p(k) \equiv \ln \Phi_p(k), \tag{25}$$

and can be shown via Taylor series expansion of $\ln \Phi_p(k)$, around $\Phi_p(0) = M_0 = 1$, to take the form

$$\Psi_p(k) = \ln \langle e^{ikx} \rangle = \sum_{n=1}^{\infty} C_n \frac{(ik)^n}{n!}, \tag{26}$$

where C_n are the so-called cumulants of X. Similar to M_n, C_n can be obtained by taking the n^{th} derivative of $\Psi_p(k)$ at $k = 0$. Furthermore, the moments and the cumulants of X can be related as:

$$\begin{aligned} C_1 &= M_1, \\ C_2 &= M_2 - M_1^2, \\ C_3 &= M_3 - 3M_2M_1 + 2M_1^3, \\ C_4 &= M_4 - 4M_3M_1 - 3M_2^2 + 12M_2M_1^2 - 6M_1^4. \\ &\cdots \end{aligned} \tag{27}$$

[29] With this background, let us look at the qth-order moment of the modulus maxima of the wavelet coefficients, $|T_\psi^{\text{wtmm}}[f](x, a)|$ (as defined in equations (15) and (16)). Dropping the subscripts and superscripts except for the dependence on the scale (a) for the sake of clarity, we have:

$$\langle |T_a|^q \rangle = \langle e^{q \ln |T_a|} \rangle. \tag{28}$$

Let us consider the left side of equation (28). Since we compute the sum of the modulus maximum of the wavelet coefficients over only the maxima lines (equation (16)), we have

$$\langle |T_a|^q \rangle = \frac{1}{N_a} Z(q, a), \tag{29}$$

where N_a is the number of maxima lines at scale a, which we know is $\sim a^{-D_f}$ where D_f is the fractal dimension of the support of the singularities. Noting that $Z(q, a) \sim a^{\tau(q)}$ (where $\tau(q)$ here stands for $\tau_{\text{wtmm}}(q)$), we have

$$\langle |T_a|^q \rangle \sim \frac{1}{a^{-D_f}} a^{\tau(q)} \sim a^{\tau(q)+D_f}. \tag{30}$$

[30] This implies

$$a^{\tau(q)+D_f} \sim \langle e^{q \ln |T_a|} \rangle, \tag{31}$$

and thus

$$\left[\tau(q) + D_f\right] \ln(a) \sim \ln\left\{ \langle e^{q \ln |T_a|} \rangle \right\}. \tag{32}$$

Using equation (26), we get

$$\ln\left\{ \langle e^{q \ln |T_a|} \rangle \right\} = \ln\left\{ \langle e^{qi(\ln |T_a|/i)} \rangle \right\} = \sum_{n=1}^{\infty} C_n' \frac{(iq)^n}{n!}, \tag{33}$$

where C_n' are the cumulants of $(\ln |T_a|)/i = C_n/i^n$, C_n being the cumulants of the magnitude $\ln |T_a|$. Rearranging the

terms in equation (33), and substituting the result in equation (32) we get:

$$\sum_{n=1}^{\infty} C_n(a)\frac{q^n}{n!} \sim \left[\tau(q) + D_f\right]\ln(a), \tag{34}$$

or

$$-D_f \ln(a) + \sum_{n=1}^{\infty} C_n(a)\frac{q^n}{n!} \sim \tau(q)\ln(a), \tag{35}$$

where

$$\begin{aligned} C_1(a) &\equiv \langle \ln|T_a|\rangle \sim c_1 \ln(a), \\ C_2(a) &\equiv \langle \ln^2|T_a|\rangle - \langle \ln|T_a|\rangle^2 \sim -c_2 \ln(a), \\ C_3(a) &\equiv \langle \ln^3|T_a|\rangle - 3\langle \ln^2|T_a|\rangle\langle \ln|T_a|\rangle + \langle \ln|T_a|\rangle^3 \sim c_3 \ln(a), \\ &\cdots \end{aligned} \tag{36}$$

[31] It is then easy to see that:

$$\begin{aligned} \tau(q) &= -D_f\ \frac{q^0}{0!} + \sum_{n=1}^{\infty}\left[\frac{C_n(a)}{\ln(a)}\right]\frac{q^n}{n!} \\ &= -c_0 + c_1 q - c_2 q^2/2! + c_3 q^3/3! \cdots \end{aligned} \tag{37}$$

where the coefficients $c_n > 0$ are estimated as the slope of $C_n(a)$ versus $\ln(a)$ ($n = 1, 2, 3 \cdots$), and $c_0 = D_f$.

[32] The implication of the above developments is that one can estimate $\tau(q)$ from the polynomial expansion of equation (37), where the coefficients of the expansion are obtained from the log-log linear regressions of the cumulants of the "magnitude" $C_n(a)$ versus $\ln(a)$ [*Delour et al.*, 2001]. It is noted that in the case of a monofractal (linear $\tau(q)$), only two linear regressions are needed in order to estimate c_0 and c_1, while in the case of a multifractal, a quadratic $\tau(q)$ approximation would need only three such linear regressions, and so forth. Comparing with the standard structure function or wavelet-based multifractal formalism based on the partition function, the efficiency of the cumulant-based multifractal analysis becomes apparent.

[33] It is of interest to understand how the coefficients c_n relate to the spectrum of singularities $D(h)$. It can be shown that [*Castaing et al.*, 1993; *Malecot et al.*, 2000; *Delour et al.*, 2001] the c_n coefficients control the way the PDF of singularities $h(x)$ (treated as random variables) shrinks to a delta distribution $\delta(h - c_1)$, where $c_1 = \langle h\rangle$, when $a \to 0$. Indeed, the cumulants of this PDF go to zero as $c_n/(\ln(1/a))^{n-1}$ for $n \geq 2$ (large deviations theory; see *Frisch* [1995]). This is an alternative statistical point of view of the Legendre Transform (geometrical point of view), which relates $\tau(q)$ and $D(h)$. Finally, it is noted that for a log-normal multifractal process for which $\tau(q)$ and $D(h)$ are quadratic, all the c_n are zero for $n \geq 2$ and $D(h)$ can be shown to be (see Appendix B):

$$D(h) = c_0 - \frac{(h - c_1)^2}{2c_2}, \tag{38}$$

with

$$h_{\min,\max} = c_1 \mp \sqrt{2c_2 c_0}, \tag{39}$$

being the limiting values of h at which $D(h) = 0$ (note that $D(h)$, being a dimension, cannot be negative). The corresponding limiting values of q for the $\tau(q)$ curve can be obtained via the Legendre transform, and are:

$$q^*_{\pm} = \pm\sqrt{\frac{2c_0}{c_2}}, \tag{40}$$

implying a linear-effect behavior of $\tau(q)$ with a slope of $h_{\min}$ (respectively, $h_{\max}$) for values of $q > q^*_+$ (respectively, $q < q^*_-$). Note that in a traditional moments-based approach, the computation of higher-order moments is guided only by issues of statistical convergence of moments, and not by theoretical considerations (i.e., the underlying multifractal nature of the process) which, as shown above, impose limits on q, beyond which $\tau(q)$ is inherently linear. Thus the cumulant-based methodology not only provides information about the multifractality of a process, but also explicitly provides the estimates of the limiting values of q given by equation (40).

[34] It is worth emphasizing that c_2, the so-called intermittency coefficient, determines the way the variance of the probability distribution of Hölder exponents h ($\mathcal{P}_a(h)$; see Appendix B) changes with scale; that is, it relates to the variability of singularities at any scale. Thus, if c_2 is zero (no variance), it implies that the singularity spectrum is a point or the given signal is monofractal (assuming that $c_n = 0\ \forall n \geq 2$). On the other hand, if c_2 is nonzero, the given signal has multifractal properties. Thus one does not have to compute $\tau(q)$ for a range of values of q to establish whether it is linear (monofractal signal) or nonlinear (multifractal signal). Estimating just one coefficient from one straight line fit, $C_2(a)$ versus $\ln(a)$, can establish if a given data set possesses intermittent multifractal characteristics [*Castaing et al.*, 1990, 1993; *Arneodo et al.*, 1998c, 1999; *Malecot et al.*, 2000; *Chanal et al.*, 2000].

3.2. Two-Point Magnitude Statistical Analysis

[35] In addition to the one-point WTMM statistics presented above, it is useful to study the two-point correlation function of the logs of the WTMM coefficients $\ln|T_a(x)|$, which determines the way the correlation structure of the Hölder exponents h (or singularities) changes with scale [*Arneodo et al.*, 1998a, 1998b]. Defining

$$\begin{aligned} \mathcal{C}(a,\Delta x) = \langle\ & (\ln|T_a(x)| - \langle\ln|T_a(x)|\rangle) \\ & \cdot(\ln|T_a(x+\Delta x)| - \langle\ln|T_a(x)|\rangle)\ \rangle, \end{aligned} \tag{41}$$

and seeing how this two-point correlation changes as a function of Δx at scale a, provides information about the space-scale (or timescale) structure that underlies the multifractal properties of the considered signal. For example, if $\mathcal{C}(a, \Delta x)$ is logarithmic in Δx and independent of scale a provided that $\Delta x > a$, i.e.,

$$\mathcal{C}(a,\Delta x) \sim \ln\Delta x \qquad \Delta x > a\ , \tag{42}$$

then long-range dependence is inferred. Moreover, *Arneodo et al.* [1998a, 1998b] have shown that for random

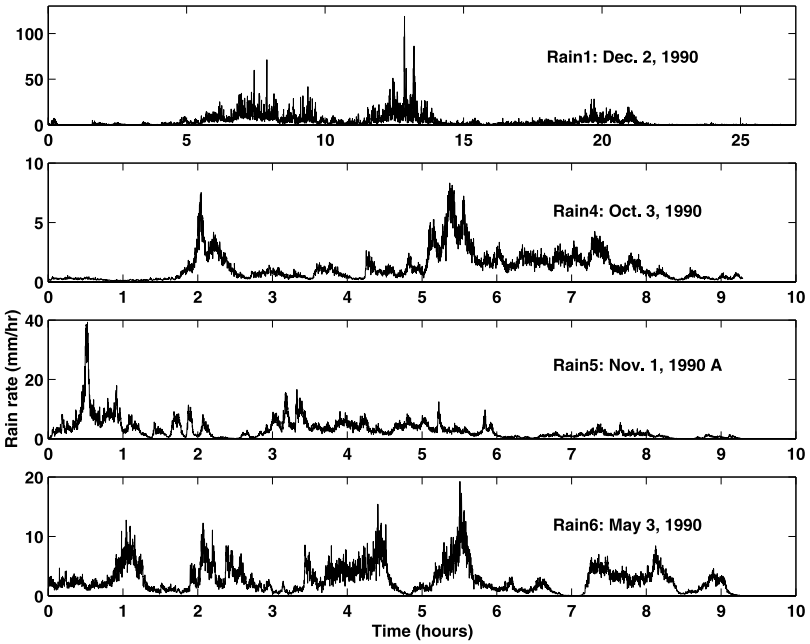

Figure 3. Time series of rainfall intensity (mm/h). Rains 4, 5, and 6 were sampled at 5 s, while Rain 1 was sampled at 10 s.

multiplicative cascades on wavelet dyadic trees [see also *O'Neil and Meneveau*, 1993]:

$$\mathcal{C}(a, \Delta x) \sim -c_2 \ln \Delta x, \tag{43}$$

where the proportionality coefficient c_2 is the same as the proportionality coefficient of $C_2(a)$ (defined in equation (36)) versus $\ln(a)$, i.e.,

$$\mathcal{C}(a, \Delta x = 0) \equiv C_2(a) \sim -c_2 \ln(a). \tag{44}$$

By computing $\mathcal{C}(a, \Delta x)$ from equation (41) and plotting it as a function of $\ln \Delta x$, inferences can be made about long-range dependence and consistency with a multiplicative cascading process. Note that the presence of multifractality does not necessarily imply either long-range dependence or multiplicative cascade [*Arneodo et al.*, 1999]. For example, one can have scaling in $C_2(a)$, with $C(a, \Delta x)$ rapidly decreasing to zero (no long-range dependence) or with $C(a, \Delta x)$ linear in $\ln \Delta x$ (long-range dependence) with a slope different than c_2, or with a slope equal to c_2 (signature of a multiplicative cascade). In making inference from a data set, it is often helpful to superimpose on the same plot the curves $\mathcal{C}(a, \Delta x)$ versus $\ln \Delta x$ for several $\Delta x > a$ and the $C_2(a)$ versus $\ln(a)$ curve and see whether their slopes agree as a consistent estimate of the intermittency coefficient c_2. This will be illustrated later in the analysis of the rainfall series.

4. Multifractal Analysis of Rainfall Intensity Series

[36] The high-resolution temporal rainfall series analyzed in this work have been collected at the Iowa Institute of Hydraulic Research, University of Iowa, with specially calibrated instrumentation that allows high-resolution sampling. Further details about the instrumentation and other auxiliary data such as wind speed, pressure, etc., collected at the same site are given by *Georgakakos et al.* [1994].

[37] In this work, we report results from analysis of four events that occurred during the period of May 1990 through April 1991. It is noted that the sampling interval of all the storms is 5 s except for the storm on 2 December 1990 which has a 10 s sampling interval. The maximum rainfall rates in these events range from 10 to 120 mm h^{-1}, the average rain rates range from 0.38 to 3.9 mm h^{-1} and the coefficients of variation range from 0.75 to 2. The rainfall time series are shown in Figure 3, and a summary of the basic statistics shown in Table 1. The notation of Rains 1, 4, 5, and 6 has been used to remain consistent with the names of the events at the ftp site (which is used world wide). The original notation was made in the order of decreasing signal length.

[38] We first present an exhaustive step-by-step analysis of one of the storms (Rain 6) as an illustration of the intricacies involved in the methodology and as a demonstration that without a priori knowledge of the signal, a reliable multifractal analysis is the result of an iterative process between diagnosis and estimation until robustness is achieved. In Figure 4, we illustrate how the continuous wavelet transform is able to filter out the nonstationarities of

Table 1. Statistics of Rain 1, 4, 5 and 6, the Events Analyzed in This Work

	Number of Samples	Mean, mm/h	Standard Deviation, mm/h
Rain 1 (2 Dec. 1990)	9696	3.9	6.2
Rain 4 (3 Oct. 1990)	6689	1.2	1.2
Rain 5 (1 Nov. 1990 A)	6689	3.0	3.4
Rain 6 (3 May 1990)	6661	2.7	2.2

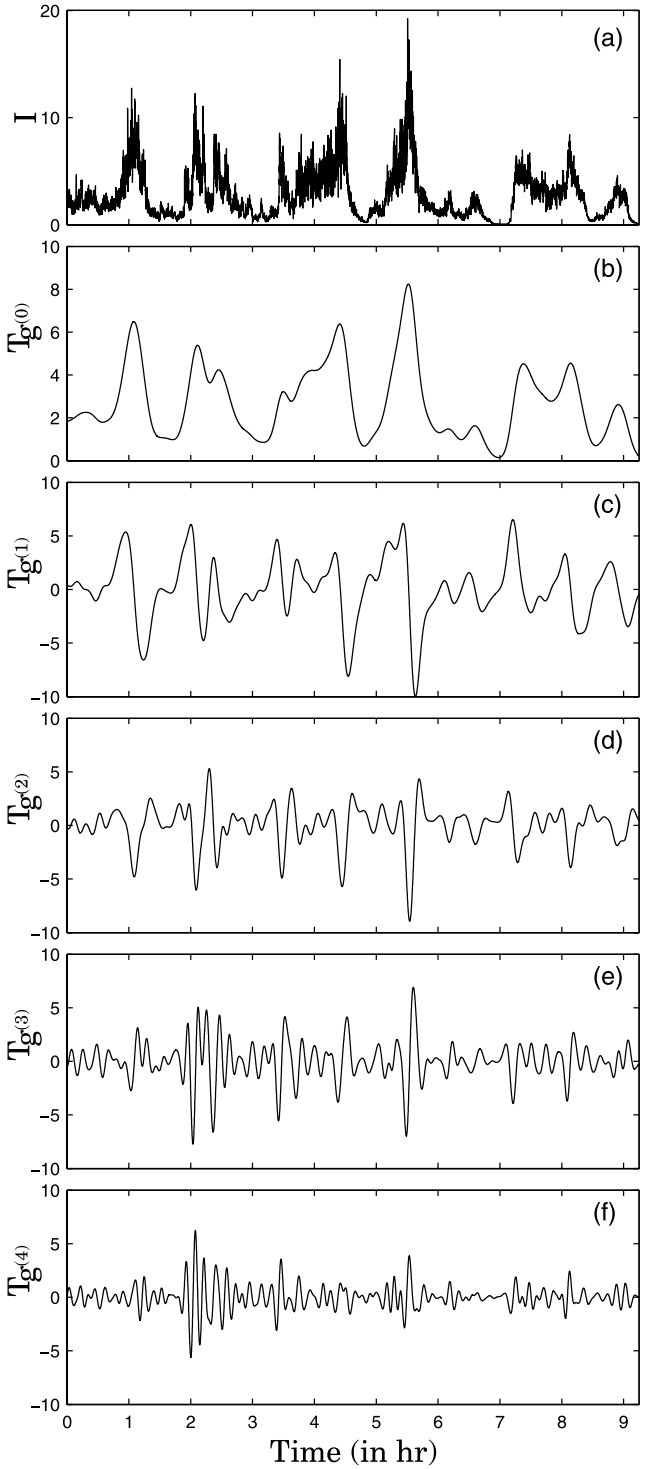

Figure 4. (a) Rainfall (Rain 6) intensity (mm/hr) versus time (hours). Rainfall intensity filtered at scale a = 742s with (b) $g^{(0)}$, (c) $g^{(1)}$, (d) $g^{(2)}$, (e) $g^{(3)}$ and (f) $g^{(4)}$. The analyzing functions $g^{(N)}$ are defined in the text.

polynomial type (Figure 4a) when using an analyzing wavelet ($g^{(n)}$) of high enough order (Figures 4e and 4f). We then describe the results obtained from the other three storms, such that generalized inferences can be made.

[39] In terms of terminology, it is noted that the development of the multifractal formalism and the related estimation procedures was presented in the previous sections using "x" as the dependent variable, to be consistent with the terminology of the original work of Arneodo et al. However, given that we are analyzing temporal series, for the rest of the discussion, we use t instead of x.

4.1. "WTMM With Sup" on the Cumulative Rain

[40] On the basis of the technical reasons presented in the previous section, the "WTMM with sup" analysis was applied to the cumulative rainfall series. Figure 5 (top) shows the cumulative of Rain 6 along with its continuous wavelet transform (using $g^{(3)}$) (Figure 5, middle), and the corresponding WTMM skeleton (Figure 5, bottom). The partition function was computed using equation (16) for various values of q ($q = -1$ to 4 in increments of 0.2) and some example plots (for $q = -1, -0.6, 0, 1, 2$ and 3) are

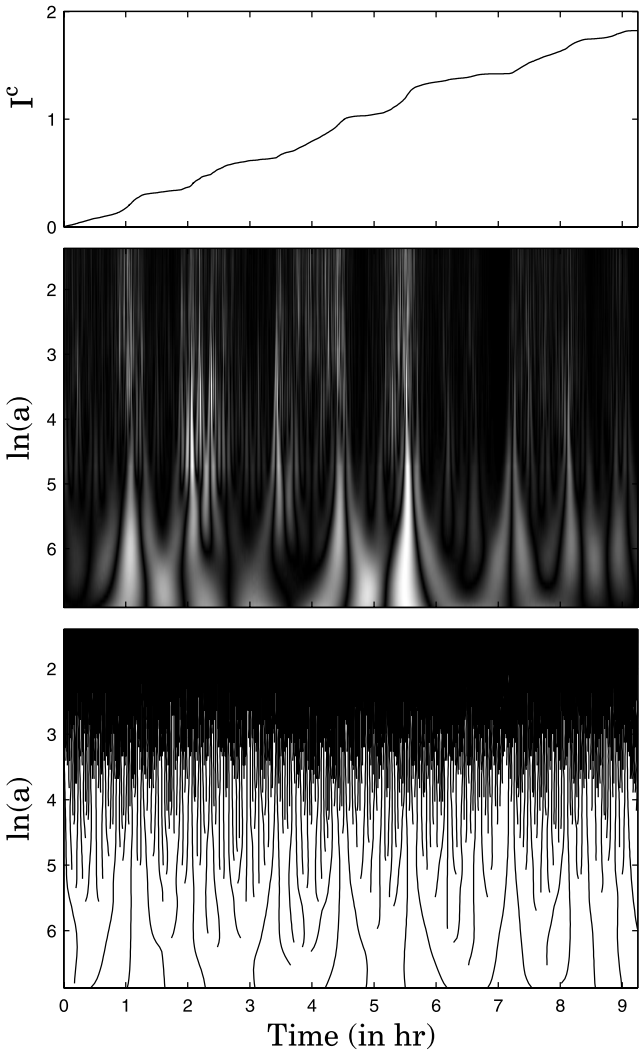

Figure 5. (top) Cumulative rainfall (Rain 6) (in 10^4 mm/hr) versus time (hours). (middle) Timescale wavelet transform representation of cumulative rainfall with the analyzing wavelet $g^{(3)}$. The modulus of the wavelet transform is coded, independently at each scale a, using 64 gray levels from black ($|T_{g^{(3)}}(t, a)| = 0$) to white ($\max_t |T_{g^{(3)}}(t, a)|$). (bottom) Wavelet transform skeleton defined by the maxima lines. The scale a is expressed in sampling time (Δt = 5s) unit.

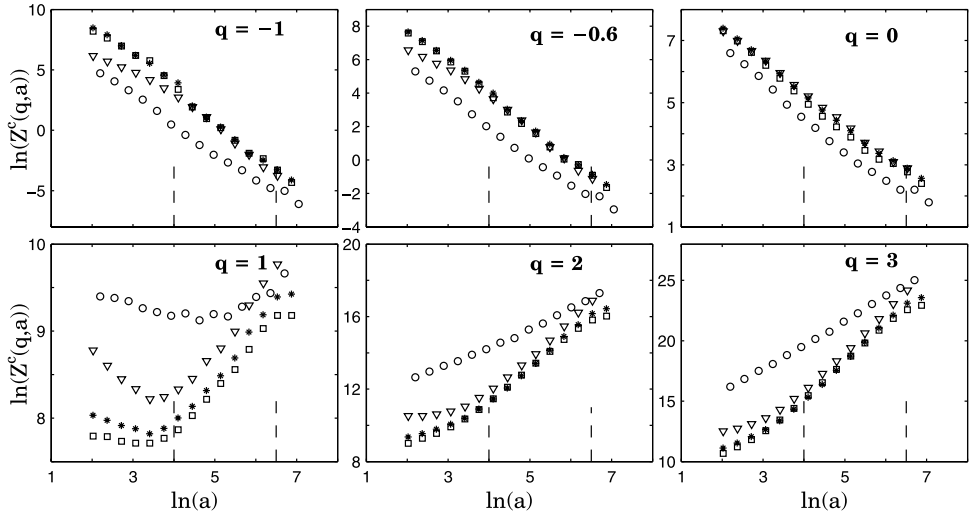

Figure 6. Moments analysis of the cumulative rainfall (Rain 6) intensity [$\ln(Z^c(q, a))$ versus $\ln(a)$: $q = -1, -0.6, 0, 1, 2, 3$] using the "WTMM with sup" method with the analyzing wavelets $g^{(1)}$ (circles), $g^{(2)}$ (squares), $g^{(3)}$ (stars) and $g^{(4)}$ (inverted triangles). The vertical dashed lines delimit the range of scales (expressed in 5s unit) used for the linear regression estimate of $\tau^c(q)$.

shown in Figure 6. It is observed that in the range of scales between $\ln(a) = 4$ ($\simeq$4–5 min) and $\ln(a) = 6.5$ ($\simeq$1 hour), one can certainly assume a log-log linearity of the moments with scale. The different symbols in Figure 6 represent analysis using wavelets of increasing order ($g^{(1)}$ through $g^{(4)}$; see Figure 1). One notices that the results obtained with $g^{(1)}$ are very different compared to those obtained using $g^{(2)}$ through $g^{(4)}$. The fact that the results obtained using $g^{(3)}$ and $g^{(4)}$ are very close to each other suggests that the proper filter to define "rainfall fluctuations" and estimate their multifractal properties is $g^{(3)}$. Using the slopes of these plots (for $q = -1$ up to 4 in increments of 0.2) and for wavelets $g^{(1)}$ through $g^{(4)}$, the spectra of scaling exponents $\tau^c(q)$ were computed (the superscript c stands for "cumulative"), and these are shown in Figure 7a, using the same symbols for each wavelet as in Figure 6. As anticipated from Figure 6, the $\tau^c(q)$ curve obtained from $g^{(1)}$ (equivalent to a structure function analysis) is misleading, while the estimate with $g^{(3)}$ can be considered as an accurate and robust estimate. By taking the Legendre transform of $\tau^c(q)$, we obtain the spectrum of singularities $D^c(h)$ as shown in Figure 7b. Again, we witness that using $g^{(1)}$ results in a misleading estimate of $D(h)$, since all singularities $h > 1$ are trivially underestimated to be close to $h = 1$, while the other wavelets do capture singularities of strength greater than 1. Since $g^{(2)}$ shows singularities of maximum strength $h \simeq 2$, analysis

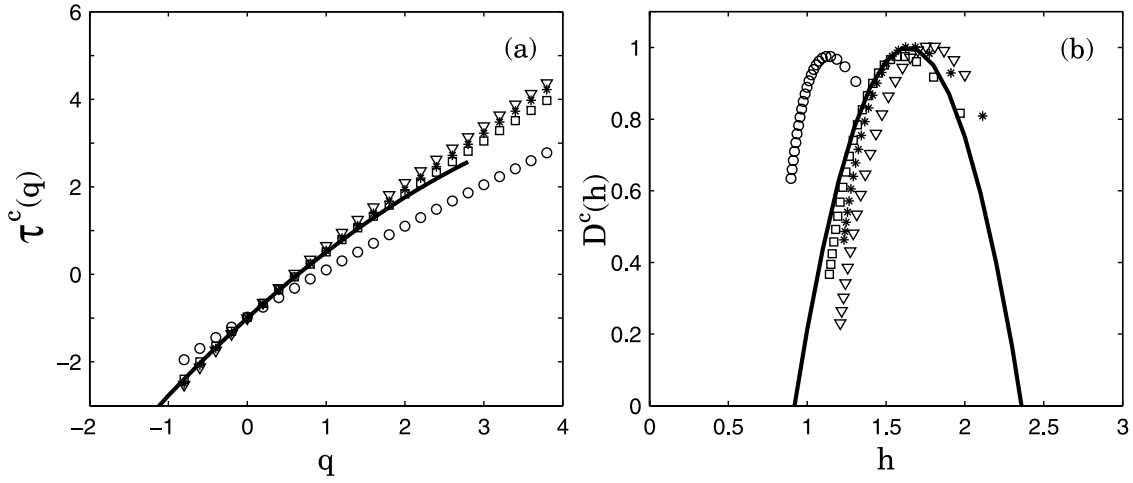

Figure 7. (a) $\tau^c(q)$ spectrum and (b) $D^c(h)$ singularity spectrum obtained for the cumulative rainfall (Rain 6) intensity using the WTMM method with the analyzing wavelets $g^{(1)}$ (circles), $g^{(2)}$ (squares), $g^{(3)}$ (stars) and $g^{(4)}$ (inverted triangles). The solid lines correspond to the spectra obtained using the cumulant method with $g^{(3)}$ ($c_0{}^c = 1$, $c_1{}^c = 1.64$, $c_2{}^c = 0.26$ and $c_3{}^c = 0$). Note that the solid line corresponding to $\tau(q)$ in Figure 7a is shown only up to $q^{\ddagger} \approx 3$ (see text for details).

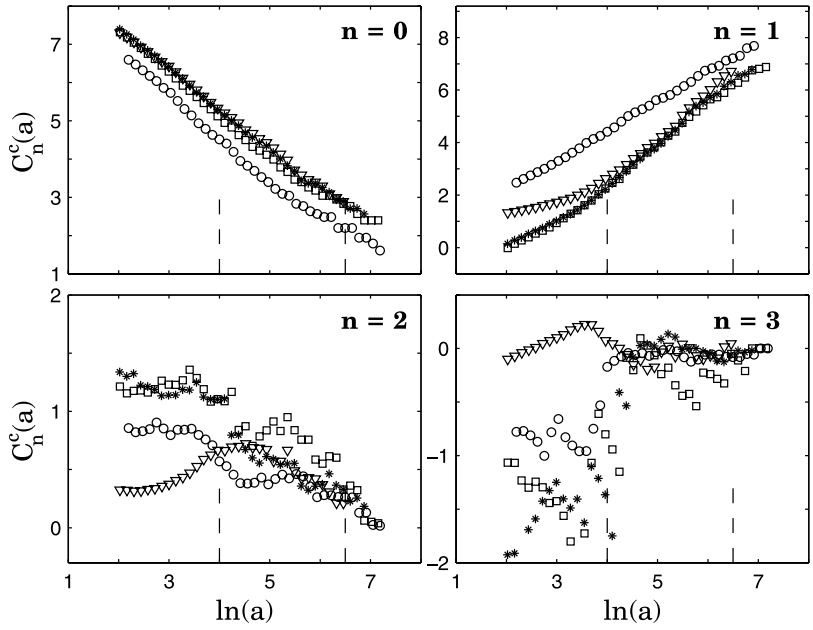

Figure 8. Cumulant analysis of the cumulative rainfall (Rain 6) intensity [$C_n^c(a)$ versus ln(a): n = 0, 1, 2, 3] using the "WTMM with sup" method with the analyzing wavelets $g^{(1)}$ (circles), $g^{(2)}$ (squares), $g^{(3)}$ (stars) and $g^{(4)}$ (inverted triangles). The vertical dashed lines delimit the range of scales (expressed in 5s unit) used for the linear regression estimate of c_n^c.

with $g^{(3)}$ and $g^{(4)}$ is prudent. The results from $g^{(3)}$ and $g^{(4)}$ confirm that the singularity spectrum has singularities of strength h greater than 2, but less than 3, thus confirming that $g^{(3)}$ is the proper wavelet for this signal.

4.2. Cumulant Analysis on the Cumulative Rain

[41] Having seen the WTMM partition function approach, we turn our attention to the alternate cumulant analysis methodology. The first-, second- and third-order cumulants were computed using equation (36) and are plotted versus ln(scale) in Figure 8. Once again, we note that the results obtained using $g^{(1)}$ as the analyzing wavelet are different from those obtained using $g^{(2)}$ through $g^{(4)}$. Similar to the partition function approach, the results using $g^{(3)}$ and $g^{(4)}$ are very close to each other. Fitting log-log straight lines between the range of scales ln(a) = 4 to 6.5, the estimated coefficients, c_0^c, c_1^c, c_2^c and c_3^c are summarized in Table 2 for all analyzing wavelets. Using the coefficients corresponding to $g^{(3)}$ (c_0^c = 1.00, c_1^c = 1.64, c_2^c = 0.26 and $c_3^c \simeq 0$) and the analytical expression (37), the $\tau^c(q)$ curve was computed and is shown as a solid line in Figure 7a. It is noted that the $\tau(q)$ curve has been plotted only up to $q \approx 3$, as the limiting value of the moment order $q^{\ddagger}$ (computed from equation (40)) is 3, implying that for higher-order moments, a linear behavior of $\tau(q)$ is theoretically expected [see also *Lashermes et al.*, 2004; *Lashermes*, 2005]. As shown in Appendix B, a parabolic $\tau(q)$ results in a parabolic $D(h) = c_0 - \frac{(h-c_1)^2}{2c_2}$, and this curve is shown as a solid line in Figure 7b.

[42] It is recalled that the analysis was performed on the cumulative rain to take advantage of the estimation efficiency of the "WTMM with sup" method. To convert the results to the rainfall intensities, it is noted that $\tau^I(q) = \tau^c(q) - q$ and $D^I(h) = D^c(h+1)$ (note also that $c_0^I = c_0^c$, $c_1^I = c_1^c - 1$, $c_2^I = c_2^c$ etc.). With this in mind, one sees from Figure 7b that the cumulant analysis estimate of $D(h)$ points to the possible presence of $h \lesssim 1$ in the cumulative rainfall series or $h < 0$ in the rainfall intensities themselves. The actual presence of $h < 0$ singularities in this rather short time series calls for a more direct estimation of these singularities. As discussed in section 2, unfortunately, the "WTMM with sup" methodology does not provide access to $h < 0$ singularities, and therefore cannot be used directly on rainfall intensities. The only way to access them is via a partition function or cumulant analysis of the CWT coefficients, as opposed to the WTMM coefficients, of the rainfall intensity signal. Such an analysis has been performed and is presented below.

4.3. CWT and Cumulant Analysis on the Rainfall Intensities

[43] The CWT-based partition functions use all the (absolute) wavelet coefficients and not just the maxima lines as in the WTMM method. Thus one cannot take negative moments because the PDFs of the (algebraic) wavelet coefficients are centered at zero. Figure 9 shows the log-log plots of CWT moments versus scale for q = 1, 2, and 3, and for analyzing wavelets $g^{(0)}$, $g^{(1)}$, $g^{(2)}$ and $g^{(3)}$ (note that

Table 2. Estimates of c_n^c for the Cumulative Rainfall (Rain 6) Obtained From Cumulant Analysis Using the WTMM Method Over the Range of Scales 4–58 min[a]

	c_0^c	c_1^c	c_2^c	c_3^c
$g^{(1)}$	0.94 ± 0.05	1.11 ± 0.02	0.15 ± 0.02	∼0
$g^{(2)}$	0.95 ± 0.04	1.54 ± 0.03	0.28 ± 0.05	∼0
$g^{(3)}$	0.98 ± 0.02	1.64 ± 0.03	0.26 ± 0.04	∼0
$g^{(4)}$	1.00 ± 0.02	1.69 ± 0.06	0.24 ± 0.05	∼0

[a]The error bars were obtained from the standard deviation of the local slope fluctuations).

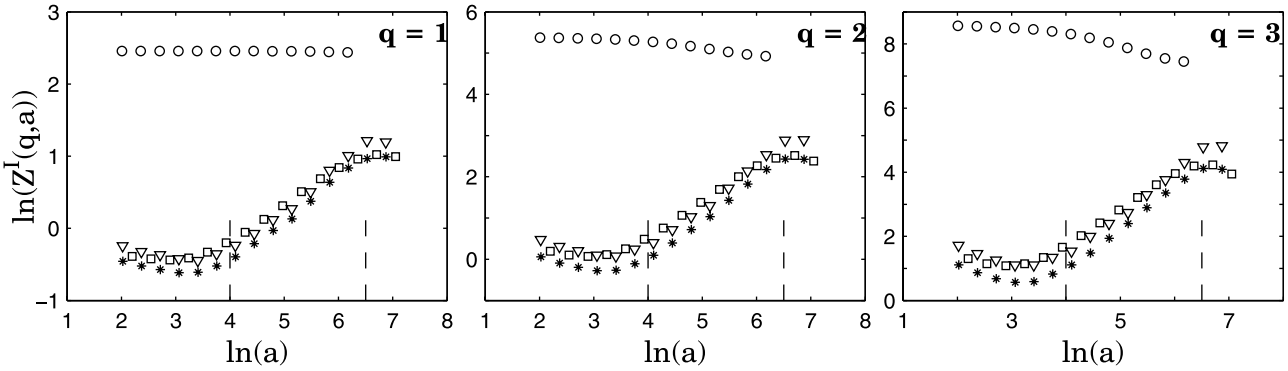

Figure 9. Moments analysis of the rainfall (Rain 6) intensity [$\ln(Z^I(q, a))$ versus $\ln(a)$: $q = 1, 2, 3$] using the CWT method with the analyzing functions $g^{(0)}$ (circles), $g^{(1)}$ (squares), $g^{(2)}$ (stars) and $g^{(3)}$ (inverted triangles). Note that the analysis with $g^{(0)}$ corresponds to the box-counting method and gives spurious results. The vertical dashed lines delimit the range of scales (expressed in 5s unit) used for the linear regression estimate of $\tau^I(q)$.

$g^{(0)}$ on the intensities is equivalent to $g^{(1)}$ on the cumulative rain). Again, log-log linearity is observed within the scales of $\ln(a) = 4$ to 6.5 and, as expected, the results with $g^{(0)}$ (equivalent to a box-counting method on rainfall intensities) are trivial. The slopes of such log-log linear plots (for $q = 0$ to 4 in intervals of 0.2) result in the $\tau^I(q)$ curve of Figure 10a, and by Legendre transform to the $D^I(h)$ curve of Figure 10b.

[44] Similarly, a cumulant analysis directly on rainfall intensities results in the plots of Figure 11 for $C_1(a)$, $C_2(a)$ and $C_3(a)$ versus $\ln(a)$. The coefficients of the linear regression lines between scales $\ln(a) = 4$ to 6.5 are summarized in Table 3. If one compares the results of "WTMM with sup" on the cumulative rainfall series using $g^{(3)}$, which give $c_1^I = 0.64 \pm 0.03$, $c_2^I = 0.26 \pm 0.04$ and $c_3^I \simeq 0$ (see Table 2) with those of the CWT directly on the intensities with $g^{(2)}$, which give $c_1^I = 0.65 \pm 0.03$, $c_2^I = 0.23 \pm 0.06$ and $c_3^I \simeq 0$ (see Table 3), the robustness of the estimates is satisfactory. Using the CWT estimates and the $\tau(q) = -c_0 + c_1\, q - c_2\, q^2/2! + c_3 q^3/3!$ expression, the $\tau^I(q)$ and $D^I(h)$ spectra are obtained and shown as solid lines in Figure 10. Note again that the $\tau^I(q)$ curve (from the cumulant computations) is shown only up to $q \approx 3$ (following equation (40)). In agreement with the "WTMM with sup" analysis on the cumulative rainfall series (which showed $h \lesssim 1$), the CWT analysis directly on rainfall intensities confirms the possible presence of singularities of strength $h \lesssim 0$ (Cantor-type sets of points) in rainfall intensity fluctuations. Unfortunately, as mentioned before, the observed domain $-0.1 \lesssim h < 0$ is so tiny that in regards of statistical convergence issues, one

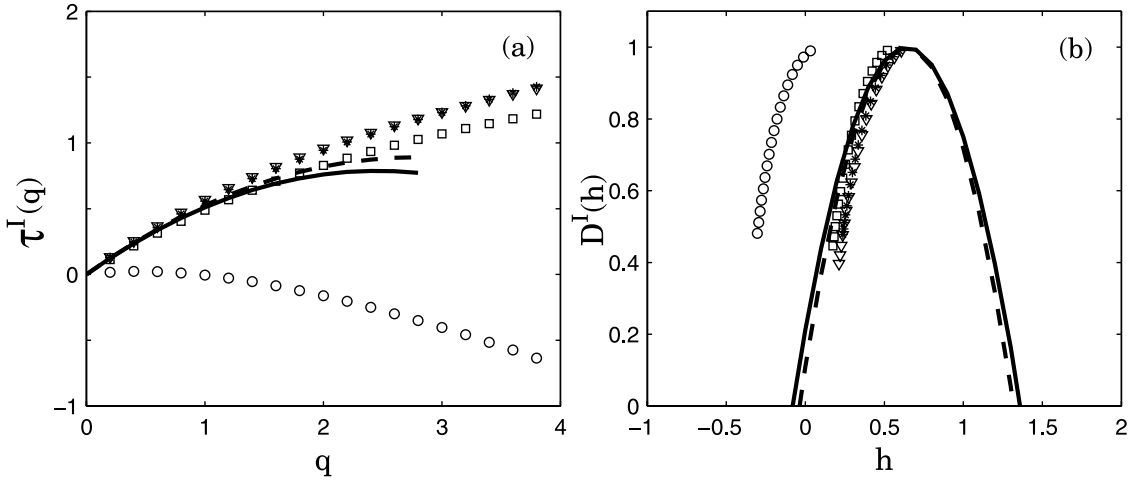

Figure 10. (a) $\tau^I(q)$ spectrum and (b) $D^I(h)$ singularity spectrum obtained with moments of the rainfall (Rain 6) intensity using the CWT method with the analyzing functions $g^{(0)}$ (circles), $g^{(1)}$ (squares), $g^{(2)}$ (stars) and $g^{(3)}$ (inverted triangles). The dashed lines correspond to the spectra of rainfall intensity obtained using the cumulant method with $g^{(2)}$ ($c_0^I = 1$, $c_1^I = 0.65$, $c_2^I = 0.23$ and $c_3^I = 0$). The solid lines correspond to the spectra in Figure 7 (obtained from the estimates of c_n^c), via the relation $\tau^I(q) = \tau^c(q) - q$ and $D^I(h) = D^c(h + 1)$, respectively. Note that the solid and dashed lines corresponding to $\tau(q)$ in Figure 10a are shown only up to $q_+^* \approx 3$ (see text for details).

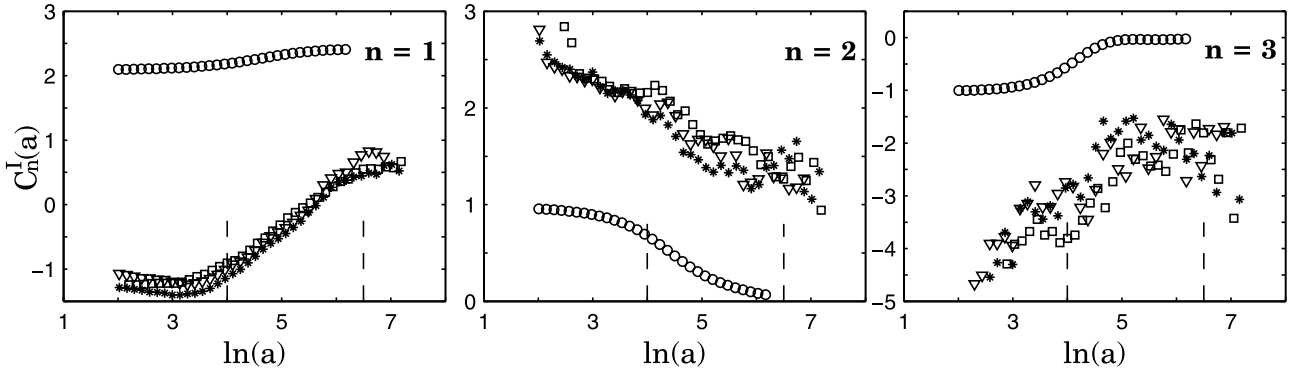

Figure 11. Cumulants analysis of the rainfall (Rain 6) intensity [$C_n^I(a)$ versus ln(a): n = 1, 2, 3] using the CWT method with the analyzing functions $g^{(0)}$ (circles), $g^{(1)}$ (squares), $g^{(2)}$ (stars) and $g^{(3)}$ (inverted triangles). The vertical dashed lines delimit the range of scales (expressed in 5s unit) used for the linear regression estimate of c^I_n. Again, the results of the box-counting method (i.e., using $g^{(0)}$) are spurious.

cannot state positively the actual presence of singularities stronger than discontinuities in rainfall intensity.

4.4. Summary of One-Point Multifractal Analysis

[45] Similar analysis was performed on the three other rainfall intensity series. Table 4 summarizes the c_0, c_1, c_2 and c_3 estimates obtained from the cumulant analysis on the cumulative rainfall series obtained from the linear regressions in Figure 12. Figure 13 displays the spectra of scaling exponents and spectra of singularities using $g^{(3)}$ on the cumulative rainfall using both the cumulant analysis (solid lines) and the "WTMM with sup" method (symbols). It is observed that while series Rain 4 and Rain 5 show a very similar multifractal behavior as series Rain 6, Rain 1 shows approximately the same strong intermittency as the other series ($c_2 \approx 0.3$), but a significantly more singular behavior, i.e., $\langle h \rangle \approx 0.1$ instead of $\langle h \rangle \approx 0.5$–$0.7$ for the other series. What physical mechanisms drive the multifractal structure of rainfall and give rise to these differences is still an open question, and is beyond the scope of this paper.

[46] The multifractal behavior was found to hold only within the storm pulses, i.e., from scales of the order of 4–5 min up to the storm pulse duration, which was of the order of 1–2 hours for the analyzed storms. For scales less than 4–5 min, no inference on scaling can be made; much higher resolution data would be needed to establish the presence or absence of scaling. Also, for scales larger than the pulse duration, a deviation from scaling becomes apparent. However, to conclusively infer the nature of scaling (absence of scaling or presence of a different scaling regime), analysis of longer series (so that a larger number of storm pulses is available) or many more data sets (which can serve as ensembles) would be needed.

5. Two-Point Magnitude Analysis of Rainfall Intensities

[47] The two-point WTMM magnitude correlation analysis of Rain 6, Rain 5, Rain 4 and Rain 1 is shown in Figure 14. On the left are the two-point correlation functions $\mathcal{C}(a, \Delta t)$ versus ln Δt (equation (41), where Δx is replaced by Δt) for rainfall intensities using the CWT method with $g^{(2)}$, and on the right are the plots obtained from the analysis of the cumulative rainfall using WTMM with $g^{(3)}$. It is observed that $\mathcal{C}(a, \Delta t)$ shows a slow logarithmic decay with the time of separation Δt (equation (42)), and that the curves fall on top of each other for $\Delta t > a$, indicating the presence of long-range correlation in rainfall fluctuations.

[48] The slopes of these lines are very close to $-c_2$ (up to numerical uncertainty) as evidenced by comparison to the cumulant $\mathcal{C}_2(a)$ versus ln (a) curve shown on the same plots (open circles). This implies that the long-range dependence found in the series is consistent with both equations (43) and (44), and therefore is likely to be the signature of the existence of an underlying multiplicative cascade process. Note that as seen in Figures 14a and 14b and Figures 14c and 14d for Rain 6 and Rain 5, the statistics of the CWT coefficients are nearly Gaussian ($\mathcal{C}_2^I(a) = \pi^2/8$; see *Delour et al.* [2001]) at a scale $a \simeq 1$ hour which coincides with the time lag beyond which the WTMM magnitudes become decorrelated ($\mathcal{C}(a, \Delta t) = 0$). This scale corresponds to the

Table 3. Cumulant Analysis Estimate of c_n^I for Rainfall (Rain 6) Intensity With the CWT Method Over the Range of Scales 4–58 min

	c_1^I	c_2^I	c_3^I
$g^{(0)}$	0.10 ± 0.02	0.20 ± 0.04	∼0
$g^{(1)}$	0.54 ± 0.03	0.29 ± 0.03	∼0
$g^{(2)}$	0.65 ± 0.03	0.23 ± 0.06	∼0
$g^{(3)}$	0.70 ± 0.03	0.28 ± 0.04	∼0

Table 4. Estimates of c_n^I for Rainfall Intensity Obtained From the Cumulant Analysis of the Cumulative Rainfall Data Rain 6, Rain 5, Rain 4, and Rain 1 Using the WTMM Method With $g^{(3)}$ Over the Range of Scales 4–58 min

	c_0^I	c_1^I	c_2^I	c_3^I
Rain 6	0.98 ± 0.02	0.64 ± 0.03	0.26 ± 0.04	∼0
Rain 5	0.97 ± 0.02	0.55 ± 0.05	0.38 ± 0.05	∼0
Rain 4	0.99 ± 0.02	0.62 ± 0.03	0.35 ± 0.15	∼0
Rain 1	1.00 ± 0.02	0.14 ± 0.03	0.30 ± 0.08	∼0

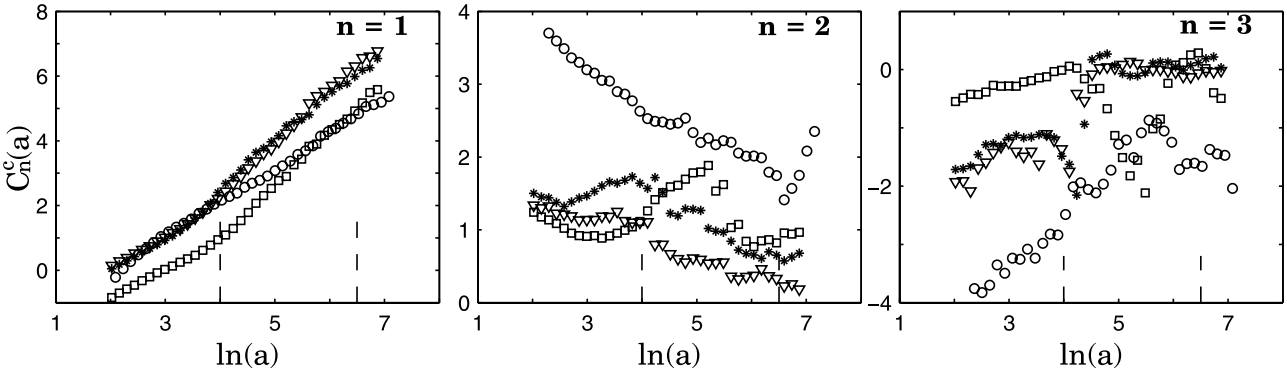

Figure 12. Cumulant analysis of cumulative rainfall intensity [$C_n^c(a)$ versus ln(a): n = 1, 2, 3] using the WTMM method with the analyzing wavelet $g^{(3)}$. The symbols correspond to the following rainfall data: Rain 1 (circles), Rain 4 (squares), Rain 5 (stars) and Rain 6 (inverted triangles). The vertical dashed lines delimit the range of scales (expressed in 5s unit) used for the linear regression estimate of c_n^c.

duration of the storm pulse, and therefore the inference is made that a multiplicative cascading mechanism is associated with rainfall fluctuations within storm pulses only, but not from one pulse to another.

[49] To further confirm the above hypothesis, the following numerical experiment was performed. First, a synthetic series from a fractionally integrated cascade (FIC) with similar multifractal properties as that found for Rain 6 (i.e., $c_0^I = 1$, $c_1^I = 0.65$, $c_2^I = 0.3$ and $c_3^I = 0$) was generated and with integral scale T = exp(9), i.e., corresponding to the whole storm duration of approximately 6 hours (see *Schertzer and Lovejoy* [1987] and *Schertzer et al.* [1997] for FIC generation). We call this "signal 1." Second, the above FIC with T = exp(9) was superimposed on the low-frequency component (LFC) of Rain 6 corresponding to the $g^{(3)}$ wavelet (see Figure 4a); we call this "signal 2." Third, on the Rain 6 low-frequency component, FIC realizations with the same multifractal structure as before but with integral timescale T' = exp(6.5), i.e., corresponding to the storm pulse duration, were superimposed next to each other; we call this "signal 3." If our hypothesis of a local cascading mechanism is correct, then the results for Rain 6 would resemble only those of "signal 3" and would differ significantly from those of "signal 1" and "signal 2." Indeed, this is the case as seen by comparing Figure 15 for the three synthetic signals and Figures 14a and 14b for Rain 6.

[50] Figure 15a shows a long-range dependence up to scale T(= exp(9)), and also scaling over the whole range T for "signal 1," as expected. Figure 15b shows a long-range dependence up to scale T (because of the integral scale of the underlying cascade), but break of scaling at the scale of the pulse duration (because of the presence of the LFC). The long-range dependence of rainfall fluctuations over the whole duration of the storm implies memory of the rainfall

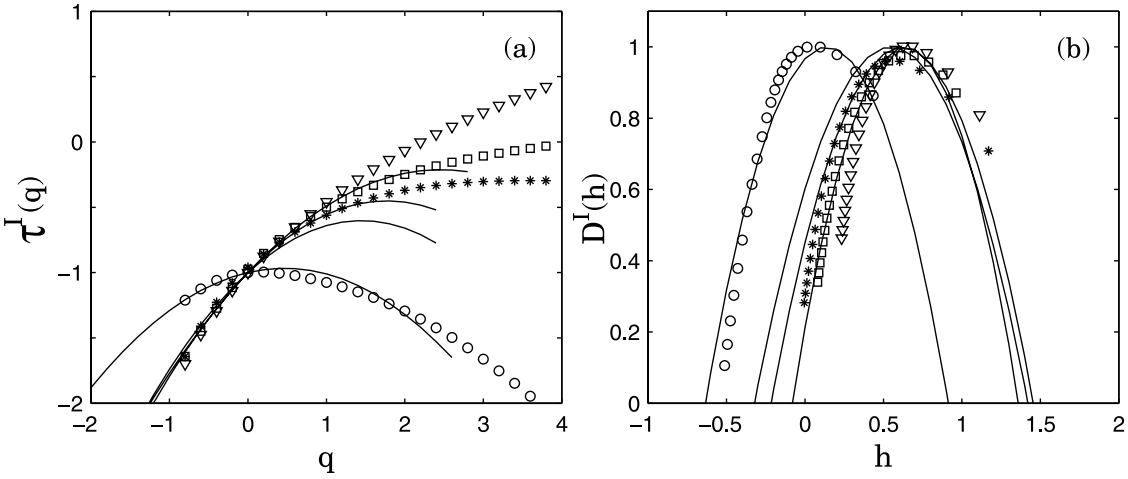

Figure 13. Multifractal spectra of rainfall intensity for Rain 1 (circles), Rain 4 (squares), Rain 5 (stars) and Rain 6 (inverted triangles) obtained from the estimates of the multifractal spectra (a) $\tau^c(q)(= \tau^I(q) + q)$ and (b) $D^c(h)(= D^I(h - 1))$ of the cumulative rainfall intensity using the WTMM method with the analyzing wavelet $g^{(3)}$. The solid lines correspond to the same spectra obtained with the cumulant method; the values of c_0^I, c_1^I, c_2^I and c_3^I are listed in Table 4. Note that the solid lines corresponding to $\tau(q)$ in Figure 13a are shown only up to $q_+^* \approx 2.4$ to 3 (see text for details).

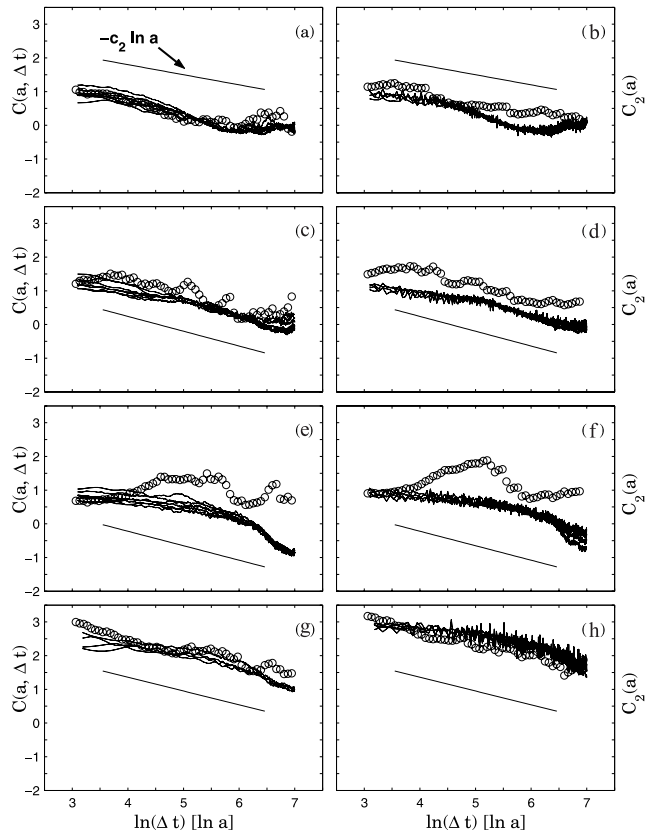

Figure 14. Two point correlation functions $\mathcal{C}(a, \Delta t)$ versus $\ln(\Delta t)$ (equation (41)) for rainfall intensity using the CWT method with $g^{(2)}$ (left column) and for cumulative rainfall intensity using WTMM with $g^{(3)}$ (right column). Each curve (solid line) corresponds to a different scale a within the scaling range. Shown are (a and b) Rain 6, (c and d) Rain 5, (e and f) Rain 4 and (g and h) Rain 1. For comparison is shown (in circles) the behavior of the corresponding second-order cumulant $C_2^I(a)$ (left column) and $C_2^c(a)$ (right column) versus $\ln(a)$. Note that for the CWT estimate of $C_2^I(a)$ we have actually plotted $C_2^I(a) - \pi^2/8$ (see text). In each panel, the straight solid line corresponds to the estimated slope $-c_2$ of the corresponding second-order cumulant (see Table 4).

fluctuations from one storm pulse to another (as in fact expected because of the FIC spanning the whole signal). Figure 15c shows a long-range dependence and also scaling only up to the storm pulse duration (timescale = T' = exp(6.5)). This implies that there is no memory from one storm pulse to another (as in fact expected because of the local FICs). This numerical experiment provides further confidence of the hypothesis for a local cascading mechanism associated with rainfall fluctuations within each storm pulse, but not throughout the storm duration.

6. Evolution of the PDF Shape Over Scales

[51] One of the by-products of scaling in rainfall fluctuations is the knowledge of how to estimate the PDF at one scale from that of another scale, i.e., how to rescale the PDF across scales. This can have practical implications in downscaling [e.g., see *Perica and Foufoula-Georgiou*, 1996; *Venugopal et al.*, 1999], or can serve as an additional verification that indeed the inferred multiscaling and the estimated multifractal spectra are correct, if the appropriately rescaled PDFs collapse on each other. The purpose of this section is to (1) present theoretical background on the wavelet-based PDF rescaling in multifractal signals [*Arneodo et al.*, 1997b, 1998c] and (2) illustrate the application of the methodology for rainfall and corroborate the accuracy of the previously obtained multifractal spectra.

[52] It is recalled that for an almost everywhere singular monofractal function, the linear spectrum $\tau(q) = qH - 1$ implies that all the points of the signal have the same local Hölder exponent: $h(x) = H$, $\forall x$. In this case, the PDF of the WTMM coefficients T_a at scale a, denoted by $\mathcal{P}_a(T)$ has been shown to relate to that at another scale $a' = \lambda a$ via [see *Arneodo et al.*, 1997b].

$$\mathcal{P}_a(T) = \left(\frac{a'}{a}\right)^{-H} \mathcal{P}_{a'}\left(\left(\frac{a'}{a}\right)^{-H} T\right). \tag{45}$$

In other words, the shape of the PDF of T_a does not depend on scale provided that we appropriately normalize the WTMM coefficients. *Castaing et al.* [1990] proposed a generalization of equation (45) for multifractals by

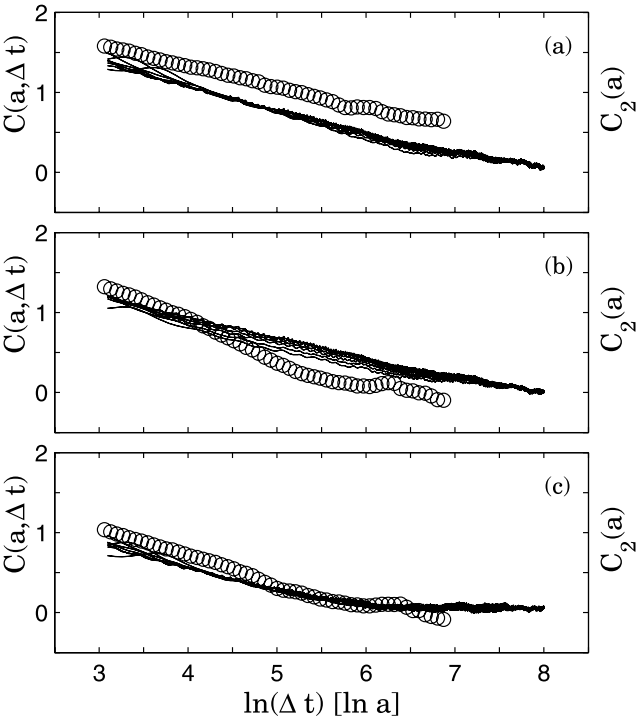

Figure 15. Two point magnitude correlation functions $\mathcal{C}(a, \Delta t)$ versus $\ln(\Delta t)$ obtained using the CWT method with $g^{(3)}$ for (a) fractionally integrated cascade (FIC) of integral timescale T = exp(9); (b) the sum of the low frequency component of rainfall intensity (Rain 6) (Figure 4a) and the previous FIC; and (c) the same superposition as in Figure 15b but with a FIC with T' = exp(6.5). For comparison is also shown (in circles) the behavior of the corresponding second-order cumulant $C_2^I(a)$ versus $\ln(a)$.

considering that H fluctuates according to a probability density function $\rho(h)$ i.e.,

$$\mathcal{P}_a(T) = \int_{-\infty}^{\infty} \rho(h) \left(\frac{a'}{a}\right)^{-h} \mathcal{P}_{a'}\left(\left(\frac{a'}{a}\right)^{-h} T\right) dh, \quad \text{for } a' > a, \tag{46}$$

that is, the PDF at scale a can be expressed as a weighted sum of dilated PDFs at larger scales $a' > a$. Let us note that the monofractal situation (equation (45)) is recovered when assuming that $\rho(h) = \delta(h - H)$ in equation (46). By denoting $u = h \ln(a)$ and $G_{aa'}(u) = \rho(\frac{u}{\ln \lambda})/\ln \lambda$, where $\lambda = \frac{a'}{a}$, the above expression can be rewritten as:

$$\mathcal{P}_a(T) = \int_{-\infty}^{\infty} G_{aa'}(u) e^{-u} \mathcal{P}_{a'}(e^{-u} T) du \quad \text{for } a' > a, \tag{47}$$

i.e., as a convolution-type equation, where the kernel G for any decreasing sequence of scales $(a_1, \cdots a_k)$ satisfies the composition law

$$G_{a_n a_1} = G_{a_n a_{n-1}} \otimes \cdots \otimes G_{a_2 a_1}, \tag{48}$$

where $\otimes$ denotes this convolution product. The kernel $G_{aa'}(u)$ is called the propagator and depends only on u (a random variable here) and a, a'.

[53] Now from the definition of the partition function $Z(q, a)$ (equations (15) and (16)), it is easy to see that

$$Z(q, a) = \int_0^{\infty} |T|^q \mathcal{P}_a(|T|) d(|T|), \tag{49}$$

where $\mathcal{P}_a(|T|)$ is the WTMM PDF at scale a, can be reexpressed, using equation (47), in the following form:

$$Z(q, a) = \int_0^{\infty} |T|^q \left(\int_{-\infty}^{\infty} G_{aa'}(u) e^{-u} \mathcal{P}_{a'}(e^{-u}|T|) du \right) d(|T|). \tag{50}$$

With the change of variable $T' = e^{-u} |T|$, one gets

$$\begin{aligned} Z(q, a) &= \left(\int_{-\infty}^{\infty} e^{qu} G_{aa'}(u) du \right) Z(q, a'), \\ &= \Phi_{G_{aa'}}(k = -iq) Z(q, a'), \end{aligned} \tag{51}$$

where $\Phi_{G_{aa'}}$ is the moment generating function (equation (22)) of $G_{aa'}$. In fact, *Arneodo et al.* [1997b] propose to estimate G as

$$\Phi_{G_{aa'}}(k = -iq) = Z(q, a)/Z(q, a') = (a/a')^{\tau(q)}. \tag{52}$$

This demonstrates that the $\tau(q)$ multifractal spectrum is directly related to the cumulant generating function (equation (25)) of the propagator $G_{aa'}$:

$$\Psi_{G_{aa'}}(-iq) = \sum_{n=0}^{\infty} C_n (a/a') \frac{q^n}{n!} = \tau(q) \ln(a/a'), \tag{53}$$

where we have used equations (33)–(37).

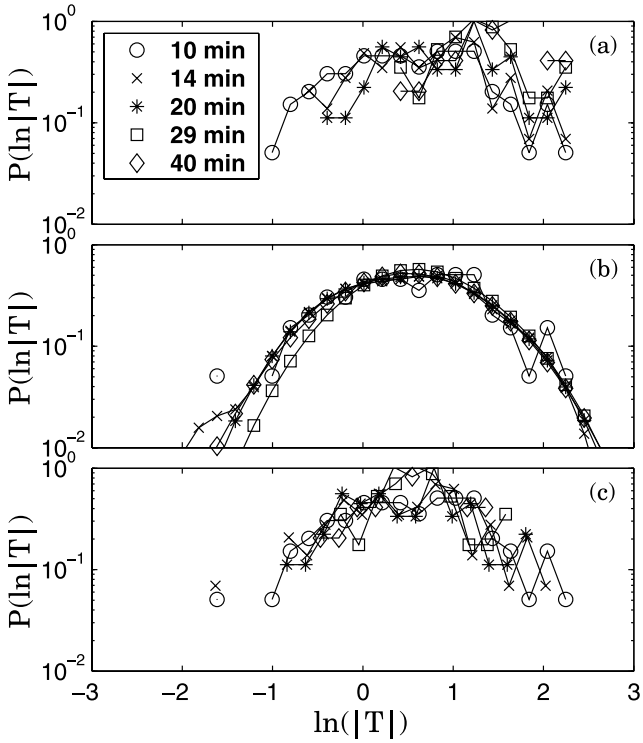

Figure 16. Demonstration of PDF rescaling via the propagator: (a) Original PDFs of the logs of WTMM coefficients (magnitude coefficients) of Rain 6 at scales ln a = {4.8, 5.14, 5.49, 5.84 and 6.18} corresponding to {10, 14, 20, 29 and 40 min}; (b) rescaled PDF using the multifractal estimates of the cumulant c_0 = 1, c_1 = 0.64; c_2 = 0.26; and (c) rescaled PDFs using an erroneous monofractal estimate of c_0 = 1 and c_1 = 0.64 clearly depicting the wrong inference.

[54] The reader is referred to *Arneodo et al.* [1997b, 1998c, 1999] for test applications of this estimation method to synthetic turbulence data. The WTMM partition function $Z_{\text{wtmm}}(q, a)$ has been computed for the Rain 6 series for scales a corresponding to the exp of {4.8, 5.14, 5.49, 5.84 and 6.18}, and using the values of $c_0 = 1$, $c_1 = 0.64$, and $c_2 = 0.26$ (see Table 4). Then via equation (52), the propagator $G_{aa'}(u)$ has been estimated and the PDFs at scales larger than exp(4.8) have been rescaled to that at scale exp(4.8) using equation (46). Figure 16a shows the original WTMM PDFs at those scales and Figure 16b shows the rescaled PDFs. The collapse of the rescaled PDFs on each other is impressive, further establishing confidence in the estimates of the multifractal spectra. It is noted that a wrong inference of monofractality for Rain 6 (c_1 = 0.67; c_2 = 0) would simply result in translated PDFs which do not collapse to each other as seen in Figure 16c. Actually the fact that the intermittency coefficient c_2 is non zero accounts for the observed change in the width of these PDFs across scales.

7. Conclusions

[55] In this paper, we have revisited some issues relating to the inference and estimation of the multifractal nature of high-resolution temporal rainfall, using wavelet-based

methods. We have established that traditional techniques can result in spurious estimates of the spectrum of scaling exponents ($\tau(q)$) and correspondingly the singularity spectrum ($D(h)$). We introduced an alternate formalism based on magnitude cumulants that is much more efficient than the traditional moments analysis or the wavelet-based partition function formalism. We have also explored the possibility of a multiplicative cascade as the generating mechanism for these rainfall data using the two-point magnitude analysis method.

[56] On the basis of the analysis of four high-resolution temporal rainfall series collected at IIHR, the following observations can be made:

[57] 1. Rainfall fluctuations (properly defined here via a wavelet filtering) exhibit multifractality. This is evidenced by the nonzero and large value of the intermittency coefficient ($c_2 \approx 0.3$), which is an order of magnitude larger than the intermittency coefficient found for turbulent velocity fluctuations ($c_2 \approx 0.025$ [e.g., see *Frisch*, 1995, p. 25]).

[58] 2. The range of singularities is between -0.1 and 1.3, centered at $\langle h \rangle \approx 2/3$. The presence of $h > 1$ suggests that traditional techniques of estimating the singularity spectrum (for instance, using the structure function method, which cannot capture singularities $h > 1$) could yield spurious estimates of $D(h)$. It also stresses the fact that rainfall intensity series should not be analyzed as a singular measure, but as a singular function. Thus the moment scaling function on the average rainfall intensities (i.e., box-counting method) would give misleading results.

[59] 3. Multifractality is documented to hold only within storm pulses, i.e., from scales of the order of $\approx 4-5$ min to the storm pulse duration which is of the order of $\approx 1-2$ hours. For scales less than 4–5 min, no inference can be made as this would require much higher resolution data. For scales larger than the storm pulse duration, a break of scaling is observed. However, not enough storms are available to explore the nature of scaling in interstorm pulse period (absence of scaling or the onset of a new scaling regime).

[60] 4. Rainfall fluctuations exhibit long-range dependence only up to the scale of the storm pulse duration implying that there is no memory in rainfall fluctuations from one storm pulse to another. In this sense, the duration of a storm pulse can be seen as equivalent to the integral scale in fully developed turbulence.

[61] 5. The long-range dependence of within-storm-pulse rain fluctuations or, equivalently, the correlation structure of the singularities inferred by the two-point magnitude analysis, suggests the presence of an underlying multiplicative cascade process. The fact that c_3 is very close to zero is also suggestive that a lognormal cascade is a good approximation of this multiplicative process.

[62] 6. An important aspect of the analysis presented here is to note that the large value of c_2 for rainfall fluctuations (i.e., large intermittency or a wide spectrum of singularities), limits the order of moments ($q_{\pm}^{*} = \pm 3$, for the analyzed data, following equation (40)) up to which one can assess the nonlinear behavior of the $\tau(q)$ curve. Note that this limitation in the order of moments is not imposed by statistical considerations, i.e, statistical convergence, but is based on purely theoretical grounds. The practical implication is that even for a very large sample, the nature of multifractality in the process reflected in c_2 restricts the useful order of moments from which multifractality can be inferred on the basis of the $\tau(q)$ curve. This is an important observation for the hydrologic literature where the extraction of the spectrum of scaling exponents ($\tau(q)$) and the subsequent inference of multifractality from the nonlinearity of $\tau(q)$ have been done on the basis of computations of moments of order as high as 7.

[63] As a concluding remark, we note that the record length of the analyzed storms is relatively short ($\approx$6000 points), and the inferred scaling range is even smaller ($\approx$100 to 1000 points) making it thus difficult to obtain accurate estimates of the multifractal spectra. This is the reason for the different complementary analyses employed in this paper, including CWT, WTMM and cumulant analysis, using wavelets of different orders, until reliable estimates are obtained. For the four storms analyzed, three exhibit similar characteristics (Rain 4, 5 and 6), while one (Rain 1) exhibits a considerably more singular behavior (a smaller $c_1 = \langle h \rangle$) but the same degree of intermittency (same c_2). The connection of the multiscaling properties of rain to the underlying physical mechanism responsible for its formation is a long-standing problem in hydrology, but falls beyond the scope of the present paper. Progress in methodologies that can conclusively infer the multifractal structure of rainfall fluctuations from small samples (as presented in this paper) offers confidence in proceeding with a microphysical analysis of these storms (whenever data are available) in the hope to be able to eventually understand the statistical-physical connections.

Appendix A: Practical Recipe for Calculating the Singularity Spectrum of a Given Data Set

[64] Without a priori knowledge of the multifractal nature of the signal, the following approach is recommended such that access to the whole spectrum of singularities is enabled via the most efficient estimation techniques.

[65] 1. Take the cumulative of the given signal $f(x)$.

[66] 2. Choose the analyzing wavelet (start with $g^{(1)}(x)$, the first derivative of the Gaussian function).

[67] 3. Compute the continuous wavelet transform of the cumulative signal.

[68] 4. Estimate $c_0 = D_f$ from the computation of $\mathcal{Z}_{\mathrm{wtmm}}(a, 0)$.

[69] 5. Estimate the cumulants $C_1(a)$, $C_2(a)$ $\cdots$ using "WTMM with sup."

[70] 6. From the plots of $C_1(a)$, $C_2(a)$ $\cdots$ versus $\ln(a)$, estimate c_1, c_2 $\cdots$

[71] 7. Using c_0, c_1, c_2, $\cdots$, compute $\tau(q) = -c_0 + c_1 q - c_2 q^2/2 + c_3 q^3/3! - \cdots$

[72] 8. From the Legendre transform of $\tau(q)$, estimate $D(h)$

[73] 9. If $D(h)$ extends up to $h = 1$, it implies that there might be singularities of Hölder exponent $h > 1$ present in the cumulative.

[74] 10. Repeat steps 2 and 3 with higher-order wavelets ($n_\psi = 2, 3, \cdots$), and see if $D(h)$ extends up to $h_{\max} < n_\psi$. If two successive wavelets show the same results, then one can be assured that the correct $D(h)$ spectrum has been obtained. Also this wavelet defines the "fluctuations" of the process ($f * g^{(n_\psi)}(.)$) to which multiscaling applies.

[75] 11. If c_2 is significantly different from 0, the given function is multifractal.

Appendix B: Derivation of the Relation Between Cumulant Coefficients and the Moments of h for a Parabolic Singularity Spectrum $D(h)$

[76] Using equation (36),

$$C_1(a) = \langle \ln |T_a| \rangle \sim \langle \ln a^h \rangle \sim \langle h \rangle \ln a, \tag{B1}$$

since $|T_a| \sim a^h$ (see equation (9)). Similarly,

$$C_2(a) = \langle \ln^2 |T_a| \rangle - \langle \ln |T_a| \rangle^2 \sim \langle \ln a^h \ln a^h \rangle - \langle h \rangle^2 (\ln a)^2. \tag{B2}$$

Thus

$$C_2(a) \sim \left(\langle h^2 \rangle - \langle h \rangle^2 \right) (\ln a)^2. \tag{B3}$$

Thus we have expressed $C_1(a)$ and $C_2(a)$ in terms of the moments of h, the singularity strength (i.e., treating h as a random variable). The task is to express the moments of h in terms of the cumulant coefficients. Noting that the probability density function of h behaves as $a^{c_0 - D(h)}$, we get

$$\begin{aligned} \langle h \rangle &= \int h \mathcal{P}_a(h) dh \sim \int h a^{c_0 - D(h)} dh \\ &\sim \int h \exp[(c_0 - D(h)) \ln a] \, dh. \end{aligned} \tag{B4}$$

For the sake of simplicity, let us assume that the spectrum of scaling exponents is parabolic, i.e., $\tau(q) = -c_0 + c_1 q - c_2 q^2/2!$. By definition the singularity spectrum $D(h)$ is the Legendre transform of $\tau(q)$, i.e.,

$$\begin{aligned} D(h) &= \min_q [qh - \tau(q)] = \min_q \left[c_0 - (c_1 - h) q + c_2 q^2 / 2! \right] \\ &= c_0 - \frac{(h - c_1)^2}{2 c_2}. \end{aligned} \tag{B5}$$

Substituting this above expression for $D(h)$ in equation (B4), we get

$$\langle h \rangle \sim \int h \exp \left[\frac{(h - c_1)^2}{2 c_2} \ln a \right] dh \sim \int h \exp \left[\frac{-(h - c_1)^2}{2 \left(-\frac{c_2}{\ln a} \right)} \right] dh. \tag{B6}$$

Noting that the mean of the distribution is c_1 and the variance is $-c_2/\ln a$, and solving the above Gaussian integral, we get

$$\langle h \rangle = c_1, \text{ and } \langle h^2 \rangle - \langle h \rangle^2 = -c_2 / \ln a. \tag{B7}$$

Substituting these expressions into the expressions above for $C_1(a)$ and $C_2(a)$, we get

$$C_1(a) \sim \langle h \rangle \ln a \sim c_1 \ln a, \tag{B8}$$

and

$$C_2(a) \sim \left(\langle h^2 \rangle - \langle h \rangle^2 \right) (\ln a)^2 \sim -\frac{c_2}{\ln a} (\ln a)^2 \sim -c_2 \ln a. \tag{B9}$$

[77] **Acknowledgments.** This work was partially supported by NSF (grant ATM-0130394); NASA (grants NAG5-12909 and NAG5-13639); and by the National Center for Earth-Surface Dynamics (NCED), an NSF Science and Technology Center (EAR-0120914) headquartered at the University of Minnesota. The data were collected at the Hydro-Meteorology Lab of the Iowa Institute of Hydraulic Research, under the supervision of Konstantine Georgakakos. We thank Anton Kruger and Witek Krajewski for their help with the data. Computational resources were provided by the Minnesota Supercomputing Institute, Digital Technology Center, at the University of Minnesota. We also thank Daniele Veneziano and two anonymous reviewers for their detailed review of our work and helpful suggestions for improving the presentation.

References

Arneodo, A., G. Grasseau, and M. Holschneider (1988), Wavelet transform of multifractals, *Phys. Rev. Lett.*, *61*, 2281–2284.

Arneodo, A., E. Bacry, and J. F. Muzy (1995a), The thermodynamics of fractals revisited with wavelets, *Physica A*, *213*, 232–275.

Arneodo, A., E. Bacry, and J. F. Muzy (1995b), Oscillating singularities in locally self-similar functions, *Phys. Rev. Lett.*, *74*, 4823–4826.

Arneodo, A., E. Bacry, S. Jaffard, and J. F. Muzy (1997a), Oscillating singularities on cantor sets: A grand-canonical multifractal formalism, *J. Stat. Phys.*, *87*, 179–209.

Arneodo, A., J. F. Muzy, and S. G. Roux (1997b), Experimental analysis of self-similarity and random cascade processes: Application to fully developed turbulence data, *J. Phys. II*, *7*, 363–370.

Arneodo, A., E. Bacry, S. Manneville, and J. F. Muzy (1998a), Analysis of random cascades using space-scale correlation functions, *Phys. Rev. Lett.*, *80*, 708–711.

Arneodo, A., E. Bacry, and J. F. Muzy (1998b), Random cascades on wavelet dyadic trees, *J. Math. Phys.*, *39*, 4142–4164.

Arneodo, A., E. Bacry, and J. F. Muzy (1998c), Towards log-normal statistics in high Reynolds number turbulence, *Eur. Phys. J. B*, *1*, 129–140.

Arneodo, A., S. Manneville, J. F. Muzy, and S. G. Roux (1999), Revealing a lognormal cascading process in turbulent velocity statistics with wavelet analysis, *Philos. Trans. R. Soc. London, Ser. A*, *357*, 2415–2438.

Bacry, E., J. F. Muzy, and A. Arneodo (1993), Singularity spectrum of fractal signals from wavelet analysis: Exact results, *J. Stat. Phys.*, *70*, 635–674.

Cârsteanu, A., and E. Foufoula-Georgiou (1996), Assessing dependence among weights in a multiplicative cascade model of temporal rainfall, *J. Geophys. Res.*, *101*, 26,363–26,370.

Castaing, B., Y. Gagne, and E. J. Hopfinger (1990), Velocity probability density-functions of high Reynolds-number turbulence, *Physica D*, *46*, 177–200.

Castaing, B., Y. Gagne, and M. Marchand (1993), Log-similarity for turbulent flows, *Physica D*, *68*, 387–400.

Chanal, O., B. Chabaud, B. Castaing, and B. Hebral (2000), Intermittency in a turbulent low temperature gaseous helium jet, *Eur. Phys. J. B*, *17*, 309–317.

Collet, P., J. L. Lebowitz, and A. Porzio (1987), The dimension spectrum of some dynamical systems, *J. Stat. Phys.*, *47*, 609–644.

Daubechies, I. (1992), *Ten Lectures on Wavelets*, *CBMS-NSF Reg. Conf. Ser. Appl. Math.*, vol. 61, Soc. for Ind. and Appl. Math., Philadelphia, Pa.

Davis, A., A. Marshak, and W. Wiscombe (1994), Wavelet-based multifractal analysis of non-stationary and/or intermittent geophysical signals, in *Wavelets in Geophysics*, edited by E. Foufoula-Georgiou and P. Kumar, pp. 249–298, Elsevier, New York.

Deidda, R., R. Benzi, and F. Siccardi (1999), Multifractal modeling of anomalous scaling laws in rainfall, *Water Resour. Res.*, *35*, 1853–1867.

Delour, J. (2001), Processus aléatoire auto-similaire: Applications en turbulence et en finance, Ph.D. thesis, Univ. of Bordeaux I, Talence, France.

Delour, J., J. F. Muzy, and A. Arneodo (2001), Intermittency of 1D velocity spatial profiles in turbulence: A magnitude cumulant analysis, *Eur. Phys. J. B*, *23*, 243–248.

Foufoula-Georgiou, E. (1997), On stochastic theories of space-time rainfall: Some recent results and open problems, in *Stochastic Methods in Hydrology: Rain, Landforms and Floods*, *Adv. Ser. on Stat. Sci. and Appl.*

Probab., vol. 7, edited by V. Gupta et al., pp. 25–72, World Sci., Hackensack, N. J.

Frisch, U. (1995), *Turbulence*, Cambridge Univ. Press, New York.

Georgakakos, K. P., A. A. Cârsteanu, and J. A. Cramer (1994), Observation and analysis of midwestern rain rates, *J. Appl. Meteorol.*, *33*, 1433–1444.

Grassberger, P., R. Badii, and A. Politi (1988), Scaling laws for invariant measures on hyperbolic and nonhyperbolic attractors, *J. Stat. Phys.*, *51*, 135–178.

Halsey, T. C., M. H. Jensen, L. P. Kadanoff, I. Procaccia, and B. I. Shraiman (1986), Fractal measures and their singularities: The characterization of strange sets, *Phys. Rev. A*, *33*, 1141–1151.

Harris, D., M. Menabde, A. Seed, and G. Austin (1998), Breakdown coefficients and scaling properties of rain fields, *Nonlinear Processes Geophys.*, *5*, 93–104.

Holschneider, M. (1989), L'analyse d'objets fractals et leur transformation en ondelettes, Ph.D. thesis, Univ. of Aix-Marseille II, Marseille, France.

Holschneider, M., and P. Tchamitchian (1990), Regularité locale de la fonction "non-differentiable" de Riemann, in *Les Ondelettes en 1989*, *Lect. Notes in Math.*, vol. 1438, edited by P. G. Lemarié, pp. 102–124, Springer, New York.

Jaffard, S. (1989), Exposants de Hölder en des points donnés et coefficients en ondelettes, *C. R. Acad. Sci., Ser. I*, *308*, 79–81.

Jaffard, S. (1997), Multifractal formalism for functions: 1. Results valid for all functions, *SIAM J. Math. Anal.*, *28*, 944–970.

Lashermes, B. (2005), Analyse multifractale pratique: coefficients dominants et ordres critiques. Applications à la turbulence pleinement développée. Effets de nombre de Reynolds fini, Ph.D. thesis, École Normale Supérieure de Lyon, Lyon, France.

Lashermes, B., P. Abry, and P. Chanai (2004), New insights into the estimation of scaling exponents, *Int. J. Wavelets Multiresolut. Info. Processing*, *2*, 497–523.

Malecot, Y., C. Auriault, H. Kahalerras, Y. Gagne, O. Chanal, B. Chabaud, and B. Castaing (2000), A statistical estimator of turbulence intermittency in physical and numerical experiments, *Eur. Phys. J. B*, *16*, 549–561.

Mallat, S. (1989), A theory for multiresolution signal decomposition: The wavelet representation, *IEEE Trans. Pattern Anal. Machine Intell.*, *11*(7), 674–693.

Mallat, S. (1998), *A Wavelet Tour in Signal Processing*, Elsevier, New York.

Mallat, S., and W. L. Hwang (1992), Singularity detection and processing with wavelets, *IEEE Trans. Inf. Theory*, *38*, 617–643.

Marsan, D., D. N. Schertzer, and S. Lovejoy (1996), Causal space-time multifractal processes: Predictability and forecasting of rain fields, *J. Geophys. Res.*, *101*(D21), 26,333–26,346.

Menabde, M., and M. Sivapalan (2000), Modeling of rainfall time series and extremes using bounded random cascades and Lévy-stable distributions, *Water Resour. Res.*, *36*, 3293–3300.

Meneveau, C., and K. R. Sreenivasan (1991), The multifractal nature of turbulent energy-dissipation, *J. Fluid Mech.*, *224*, 429–484.

Meyer, Y. (1992), *Wavelet and Applications*, Springer, New York.

Muzy, J. F., E. Bacry, and A. Arneodo (1991), Wavelets and multifractal formalism for singular signals: Application to turbulence data, *Phys. Rev. Lett.*, *67*, 3515–3518.

Muzy, J. F., E. Bacry, and A. Arneodo (1993), Multifractal formalism for fractal signals: The structure-function approach versus the wavelet-transform modulus-maxima method, *Phys. Rev. E*, *47*, 875–884.

Muzy, J. F., E. Bacry, and A. Arneodo (1994), The multifractal formalism revisited with wavelets, *Int. J. Bifurcation Chaos*, *4*, 245–302.

Olsson, J., J. Niemczynowicz, and R. Berndtsson (1993), Fractal analysis of high-resolution rainfall time series, *J. Geophys. Res.*, *98*(D12), 23,265–23,274.

O'Neil, J., and C. Meneveau (1993), Spatial correlations in turbulence: Predictions from the multifractal formalism and comparison with experiments, *Phys. Fluids A*, *5*, 158–172.

Paladin, G., and A. Vulpiani (1987), Anomalous scaling laws in multifractal objects, *Phys. Rep.*, *156*, 147–225.

Parisi, G., and U. Frisch (1985), On the singularity structure of fully developed turbulence, in *Turbulence and Predictability in Geophysical Fluid Dynamics*, edited by M. Ghil, R. Benzi, and G. Parisi, pp. 84–88, Elsevier, New York.

Perica, S., and E. Foufoula-Georgiou (1996), Linkage of scaling and thermodynamic parameters of rainfall: Results from midlatitude mesoscale convective systems, *J. Geophys. Res.*, *101*(D3), 7431–7448.

Roux, S., J. F. Muzy, and A. Arneodo (1999), Detecting vorticity filaments using wavelet analysis: About the statistical contribution of vorticity filaments to intermittency in swirling turbulent flows, *Eur. Phys. J. B*, *8*, 301–322.

Schertzer, D., and S. Lovejoy (1987), Physical modeling and analysis of rain and clouds by anisotropic scaling multiplicative processes, *J. Geophys. Res.*, *92*(D8), 9693–9714.

Schertzer, D., S. Lovejoy, F. Schmitt, Y. Chiguirinskaya, and D. Marsan (1997), Multifractal cascade dynamics and turbulent intermittency, *Fractals*, *5*, 427–471.

Veneziano, D., R. L. Bras, and J. D. Niemann (1996), Nonlinearity and self-similarity of rainfall in time and a stochastic model, *J. Geophys. Res.*, *101*(D21), 26,371–26,392.

Venugopal, V., and E. Foufoula-Georgiou (1996), Energy decomposition of rainfall in the time-frequency-scale domain using wavelet packets, *J. Hydrol.*, *187*, 3–27.

Venugopal, V., E. Foufoula-Georgiou, and V. Sapozhnikov (1999), A space-time downscaling model for rainfall, *J. Geophys. Res.*, *104*(D16), 19,705–19,721.

A. Arneodo and S. G. Roux, Laboratoire de Physique École Normale Supérieure de Lyon 46 Allée d Italie, F-69364 Lyon Cédex 07, France. (alain.arneodo@ens-lyon.fr; stephane.roux@ens-lyon.fr)

E. Foufoula-Georgiou, St. Anthony Falls Lab, University of Minnesota, Mississippi River at 3rd Avenue SE, Minneapolis, MN 55414, USA. (efi@umn.edu)

V. Venugopal, Centre for Atmospheric and Oceanic Sciences, Indian Institute of Science, Bangalore 560012, India. (venu@caos.iisc.ernet.in)